

# Anchored-STFT and GNAA: An extension of STFT in conjunction with an adversarial data augmentation technique for the decoding of neural signals

Omair Ali<sup>1†</sup>, Muhammad Saif-ur-Rehman<sup>3,4†</sup>, Susanne Dyck<sup>1</sup>, Tobias Glasmachers<sup>2</sup>, Ioannis Iossifidis<sup>3</sup> and Christian Klaes<sup>1</sup>

<sup>1</sup>Department of Neurosurgery, Knapschaftskrankenhaus Bochum, Ruhr University Bochum, Germany, <sup>2</sup>Institute of Neuroinformatics, Ruhr University Bochum, Germany, <sup>3</sup>Institute of Informatics, University of Applied Science, Bottrop, Germany; <sup>4</sup>Department of Electrical Engineering and Information Technology, Ruhr-University Bochum

† First author (these **two authors** contributed equally.)

## Abstract

**Objective.** Brain-computer interfaces (BCIs) enable direct communication between humans and machines by translating brain activity into control commands. Electroencephalography (EEG) is one of the most common sources of neural signals because of its inexpensive and non-invasive nature. However, interpretation of EEG signals is non-trivial because EEG signals have a low spatial resolution and are often distorted with noise and artifacts. Therefore, it is possible that meaningful patterns for classifying EEG signals are deeply hidden. Nowadays, state-of-the-art deep-learning algorithms have proven to be quite efficient in learning hidden, meaningful patterns. However, the performance of the deep learning algorithms depends upon the quality and the amount of the provided training data. Hence, a better input formation (feature extraction) technique and a generative model to produce high-quality data can enable deep learning algorithms to achieve high generalization quality. **Approach.** In this study, we propose a novel input formation (feature extraction) method in conjunction with a novel deep learning based generative model to harness new training examples. The inputs (feature vectors) are formed (extracted) using a modified Short Time Fourier Transform (STFT) called anchored-STFT. Anchored-STFT, inspired by wavelet transform, tries to minimize the tradeoff between time and frequency resolution. As a result, it extracts the inputs (feature vectors) with better time and frequency resolution compared to standard STFT. Secondly, we introduce a novel generative adversarial data augmentation technique called gradient norm adversarial augmentation (GNAA) for generating more training data. Thirdly, we investigate the existence and significance of adversarial inputs in EEG data. **Main Results.** We evaluated our methods on the BCI competition II dataset III and on the BCI competition IV dataset 2b. Our approach obtained a kappa value of 0.814 for BCI competition II dataset III and 0.618 for BCI competition IV dataset 2b for session-to-session transfer on evaluation data. For BCI competition II dataset III, our approach yielded 3.9% and 1.75% improvement in kappa value over the winner algorithm and the STFT based feature extraction technique, respectively, whereas for BCI competition IV dataset 2b, our approach yielded a 3.2 % improvement in kappa value over the winner algorithm of the competition and 2.9 % improvement in accuracy over the STFT based feature extraction technique. **Significance.** The results of this study show that the proposed method (anchored-STFT) can enhance the decoding accuracy of BCI decoding applications as compared to standard STFT based feature extraction method. To the best of our knowledge, we are the first to investigate the effect of adversarial inputs on neural data by applying adversarial perturbation using a novel method.

## Introduction

Neural signals are widely used as a key source of input in the areas of medical diagnosis and rehabilitation engineering. A brain computer interface (BCI) is used to translate neural signals into command signals to control an extracorporeal robotic device (Graimann, Allison, & Pfurtscheller, 2010). Henceforth, a BCI establishes an alternative pathway of communication and control between the user and the external machine. The successful translation of neural signals into command signals plays a vital role in the rehabilitation of physically disabled people (Kübler, et al., 2009; Klaes, et al., 2015; Kellis, et al., 2010; Aflalo, et al., 2015; Ajiboye, et al., 2017; Choi, Kim, Ryu, Kim, & Sohn, 2018). The first step in this process is the recording of neural signals from the areas of the brain which process the user's intent (Klaes, et al., 2015; Pfurtscheller & Lopes da Silva, 1999; Müller-Gerking, Pfurtscheller, & Flyvbjerg, 1999; Grosse-Wentrup & Buss, 2008; Keng Ang, Yang Chin, Wang, Guan, & Zhang, 2012; Ramoser, Muller-Gerking, & Pfurtscheller, 2000; A. Mousavi, J. Maller, B. Fitzgerald, & J. Lithgow, 2011). The neural signals are recorded either by invasive (Aflalo, et al., 2015; Kellis, et al., 2010) or non-invasive methods (Pfurtscheller & Lopes da Silva, 1999; Ramoser, Muller-Gerking, & Pfurtscheller, 2000; A. Mousavi, J. Maller, B. Fitzgerald, & J. Lithgow, 2011). Invasive methods include implanting electrodes in the brain at the area of interest whereas most non-invasive BCI systems use EEG signals, i.e., the electrical brain activity recorded from electrodes which are placed on the scalp. In the next stage, the recorded signals are digitized and preprocessed using digital signal processors (DSPs), often referred as neural signal processors (NSPs). The preprocessed signals are then utilized to extract feature vectors, which are further fed to a decoding algorithm to map it to corresponding intended action. The output of the decoding algorithm is then transformed into control signal to control the external device.

Invasive methods require a surgical operation to implant electrodes in the brain, henceforth, non-invasive recording techniques are preferable among humans and more commonly used for BCI studies. EEG is one of the most common non-invasive ways of monitoring movement related signals (Nicolas-Alonso & Gomez-Gil, 2012). Movement related signals that are induced by a user from the motor cortex by imagining the motor movements without any limb movement or external stimulus is called motor imagery (MI) (Tabar & Halici, 2017; Li , et al., 2020; Fukunaga, 2013). In this study, we used EEG signals to decode and classify the MI signals into corresponding control signals. MI-EEG signal is one of the most commonly studied signals in BCI since it can be generated spontaneously by just imagining a movement without any external stimulation (A. Mousavi, J. Maller, B. Fitzgerald, & J. Lithgow, 2011; Grosse-Wentrup & Buss, 2008; Müller-Gerking, Pfurtscheller, & Flyvbjerg, 1999; Ramoser, Muller-Gerking, & Pfurtscheller, 2000). Classifying the MI-EEG signal is quite challenging due to several reasons. Firstly, it is quite weak and has low signal-to-noise ratio. Secondly, it is a non-linear and non-stationary signal.

The successful classification of a MI-EEG signal into a corresponding control signal mainly depends on feature extraction techniques and machine learning algorithms. The current state-of-the-art feature extraction algorithms include common spatial pattern (CSP) (Müller-Gerking, Pfurtscheller, & Flyvbjerg, 1999; Ramoser, Muller-Gerking, & Pfurtscheller, 2000), adaptive auto regressive (AAR) (Schlögl, Flotzinger, & Pfurtscheller, 1997), short time Fourier transform (STFT) (Tabar & Halici, 2017) and wavelet transform (WT) (Li , et al., 2020). The conventional

classifiers used to classify EEG signals (Ramoser, Muller-Gerking, & Pfurtscheller, 2000; Firat Ince, Arica, & Tewfik, 2006; Schlögl, Lee, Bischof, & Pfurtscheller, 2005) include linear discriminant analysis (LDA) (Fukunaga, 2013), Bayesian classifiers (Nielsen & Jensen, 2001) and support vector machines (SVM) (Kübler, et al., 2009; Cortes & Vapnik, 1995).

Recently, deep-learning algorithms gained popularity by producing many state-of-the-art results in several computer vision tasks (Shah, et al., 2020; Ren S. , He, Girshick, & Sun, 2017) as well as in few BCI and spike sorting studies. In (Saif-ur-Rehman, et al., 2019) a deep learning-based novel algorithm is presented that extracts the channels recording neural data, which is further enhanced by proposing a novel spike sorting pipeline in (Saif-ur-Rehman, et al., 2020). Another variant of (Saif-ur-Rehman, et al., 2019) is proposed by (Issar, C. Williamson, B. Khanna, & A. Smith, 2020), whereas deep learning-based feature extraction algorithm is proposed for online BCI decoding applications. Similarly, in (An, Kuang, Guo, Zhao, & He, 2014) a deep belief network (DBN) has outperformed SVM in the classification of EEG-MI tasks. In another study (Wulsin, Gupta, Mani, Blanco, & Litt, 2011), DBN was used to detect anomalies in the EEG signals. In (Ren & Wu, 2014), DBN was also used to extract feature vectors for the classification algorithm. Convolution neural networks (CNNs) are also successfully used for decoding in BCI applications. In (Yang, Sakhavi, K. Ang, & Guan, 2015), CNN was employed in classification of MI-EEG signals. In order to model cognitive events from EEG signals, a novel multi-dimensional feature extraction technique using recurrent convolutional neural networks was proposed in (Bashivan, Rish, Yeasin, & Codella, 2015). In (Jirayucharoensak, Pan-Ngum, & Israsena, 2014), an automatic emotion recognition using EEG data is performed by employing stacked autoencoders and two Softmax layers.

Today, algorithms based on the CNN architecture are the most successful algorithms in image recognition tasks. One reason behind this success is the translation invariance of CNN. Therefore, in a few BCI studies, algorithms to convert EEG signal into image representation are proposed. In (Yang, Sakhavi, K. Ang, & Guan, 2015), a feature extraction technique is proposed that keeps the temporal, spectral and spatial structure of EEG signal intact. In the proposed algorithm, the power spectrum of the recorded EEG signal of each electrode was estimated and then the sum of squared absolute values is calculated for three selected frequency bands. In the next stage, the polar projection method maps the location of electrodes from 3D to 2D, which yields an image like structure. In another study, the information about location, time, and frequency is combined using short time Fourier transform (STFT) to convert an EEG signal to an image structure. In (Li , et al., 2020), the EEG-MI signal is transformed into an image using a wavelet transform, only later to be used by CNN for the classification of the signal.

STFT is one of the most used methods for time-frequency analysis of a time-series signal (Sejdić, Djurović, & Jiang, 2009) and produced many state-of-the-art results for EEG decoding applications (Tabar & Halici, 2017). The fixed-length window in STFT limits it to simultaneously acquire both temporal and spectral resolution. Inspired by the wavelet transform and Faster RCNN - an object detection algorithm - we introduced an extension of STFT to address its limitations (the trade-off between spectral and temporal resolution). We named this extension “anchored-STFT”. It uses anchors of different lengths and transforms the EEG signal into an image corresponding to

each anchor, which is slid across the EEG-MI signal. It mitigates the issue of the tradeoff by obtaining the image representations of an EEG-MI signal with different temporal and spectral resolutions. These images are then used to train the deep learning algorithm to categorize the EEG-MI signal into a respective class of action.

However, the requirement of a large, labeled data set is still a challenge in training deep learning models for BCI applications, since such data sets are rare. Therefore, the generation of new meaningful inputs from existing inputs can enhance the performance of deep learning algorithms.

In this study, we additionally propose a novel data augmentation technique called gradient norm adversarial augmentation (GNAA). The proposed method automatically selects the meaningful features in a feature vector and perturbs these features in the direction of the decision boundary. As a result, it produces new and legitimate feature vectors. The gradient of the cost function with respect to a feature vector automatically selects the features in a feature vector that plays a pivotal role in classification. In this study, we showed that our proposed feature vector extraction technique (anchored-STFT) along with the proposed data augmentation technique (GNAA) can be used to enhance the performance of BCI applications. Finally, we further investigated the existence of adversarial inputs in BCI applications.

The proposed approaches are validated on the publicly available datasets: BCI Competition II dataset III and BCI Competition IV dataset 2b.

## Materials and Methods

In this study, we performed the classification of MI-EEG signals. The whole pipeline of the classification process is shown as a block diagram in **Figure 1**. It consists of three modules: Feature extraction, Data augmentation and Classification. We propose an extension of Short time Fourier Transform (STFT) for feature extraction called **anchored-STFT**. We also propose a novel data augmentation method called **Gradient Norm adversarial augmentation (GNAA)**. We also propose a novel architecture of convolutional neural network for classification called **Skip-Net**, which is inspired by residual learning framework ([He, Zhang, Ren, & Sun, 2016](#)). As we used publicly available datasets, the recording of the EEG signals is not included in the pipeline. First, the features are extracted from EEG signals using anchored-STFT.

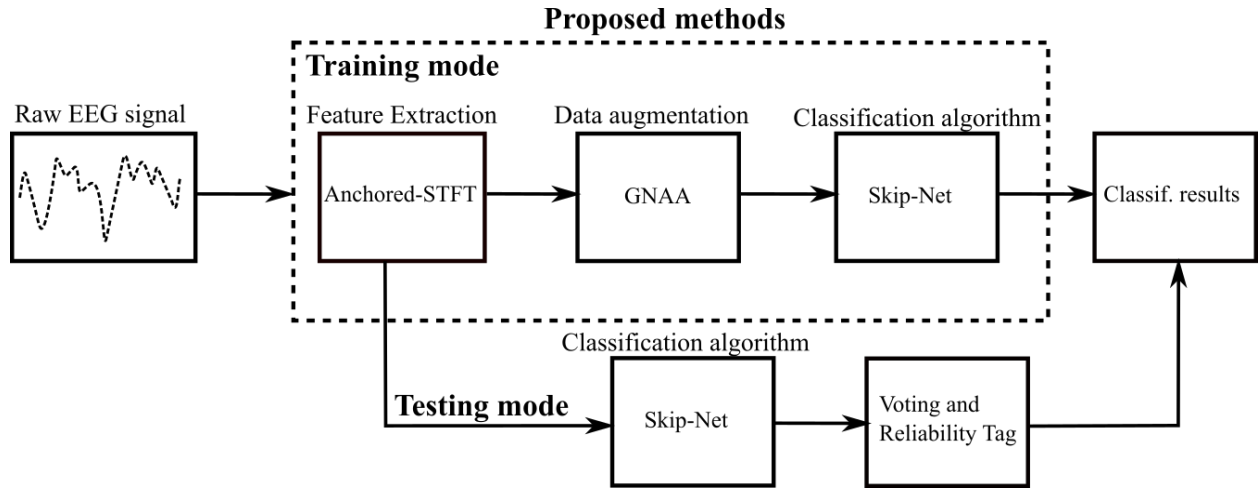


**Figure 1:** The workflow of the MI-EEG signal classification process in this study. Features are extracted from raw EEG signals using anchored-STFT. During training the GNAA method is employed on the extracted features to enhance the amount of training data to train Skip-Net algorithm. During testing, the extracted features are directly fed to the Skip-Net algorithm to perform classification and voting is done on the output of the Skip-Net algorithm to get the final classification result and its reliability tag.

The extracted features are then used by GNAA method to enhance the amount of training data for the Skip-Net algorithm in training mode. The extracted features from the anchored-STFT are directly used by the Skip-Net algorithm for classification during the testing mode. Voting is done on the output of the Skip-Net algorithm to get the final classification result. Here, the purpose of voting is to deduce the final classification result as well as the reliability of the predicted result. A detailed explanation of each of the modules of the pipeline is mentioned in sections below.

## Datasets & Preprocessing

We used the publicly available dataset III from BCI competition II ([Schlögl A. , Outcome of the BCI-competition 2003 on the Graz data set, 2003](#)) and dataset 2b from BCI competition IV ([Leeb, et al., 2007](#)) for the evaluation of our methods, since these are the benchmark datasets for EEG-MI decoding. These datasets contain the EEG recordings from 1 and 9 subjects respectively, where each subject performed left/right hand motor imagery (MI) tasks. The datasets contain the neural activity of three selected electrodes (C3, C4, Cz), which were placed on the motor areas of the brain. The dataset III from BCI competition II was recorded with a sampling frequency of 128 Hz whereas dataset 2b from BCI competition IV was recorded with a sampling frequency of 250 Hz and it was bandpass filtered between 0.5 Hz and 100 Hz and a notch filter was applied at 50 Hz. BCI competition II dataset III contains 280 trials in total, out of which 140 are training trials and the remaining 140 are test trials.

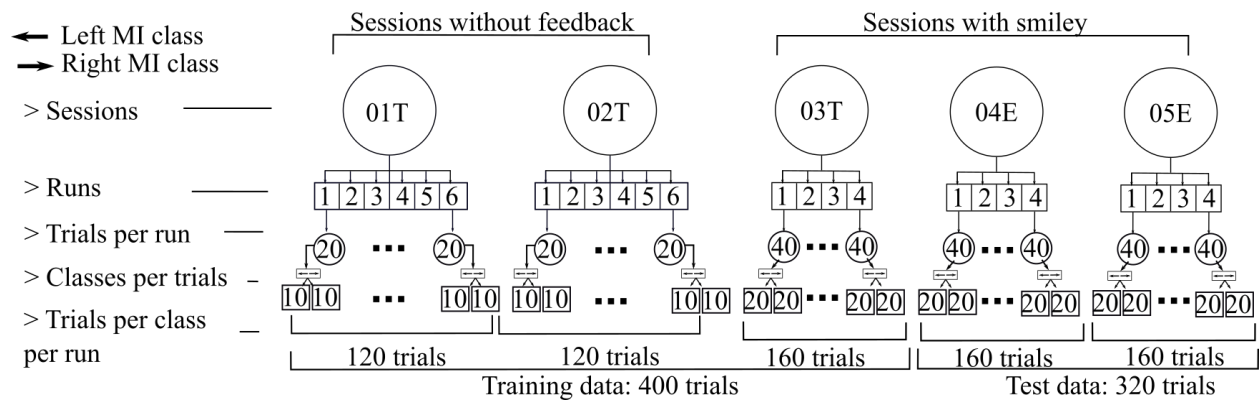


**Figure 2:** The data distribution of the dataset for each subject for training and testing the algorithm. Each subject had 5 recording sessions. Session 1 and Session 2 (01T and 02T) are without feedback. Session 3, Session 4 and Session 5 (03T, 04E and 05E) are with smiley feedback. Session 1 and Session 2 had 6 runs each. Each run had 20 trials. Out of these 20 trials, 10 trials belong to left MI class and remaining 10 trials belong to right MI class. Session 3, Session 4 and Session 5 had 4 runs each. Each run had 40 trials. Out of these 40 trials, 20 trials belong to left MI class and remaining 20 trials belong to right MI class.

In BCI competition IV dataset 2b, five sessions were recorded for each subject, whereby first two sessions (01T and 02T) are the screening sessions without feedback, whereas the remaining sessions (03T, 04E and 05E) are online feedback sessions with smiley feedback (see **Figure 2**). Three sessions (01T, 02T and 03T) were used for training and two sessions (04E and 05E) were used for evaluation purpose as recommended in the dataset description as shown in **Figure 2**. The training sessions contain a total of 400 trials, out of which 200 trials belong to left MI class and the remaining 200 trials belong to right MI class. The test sessions contain a total of 320 trials for each subject. The data distribution is shown in **Figure 2**. The experimental procedure of one trial of a screening session without feedback is shown in **Figure 3** and that of an online feedback session with smiley feedback is shown in **Figure 4**.

In screening sessions without feedback (see **Figure 3**), each trial started with a fixation cross and a short acoustic alarm tone. Few seconds later, a visual cue in form of an arrow was presented for 1.25 seconds, which pointed either to the left or right based on the class. After the cue, the subjects imagined the corresponding movement for 4 seconds. At the end of each trial, a randomized intertrial interval of 1.5-2.0 seconds was added.

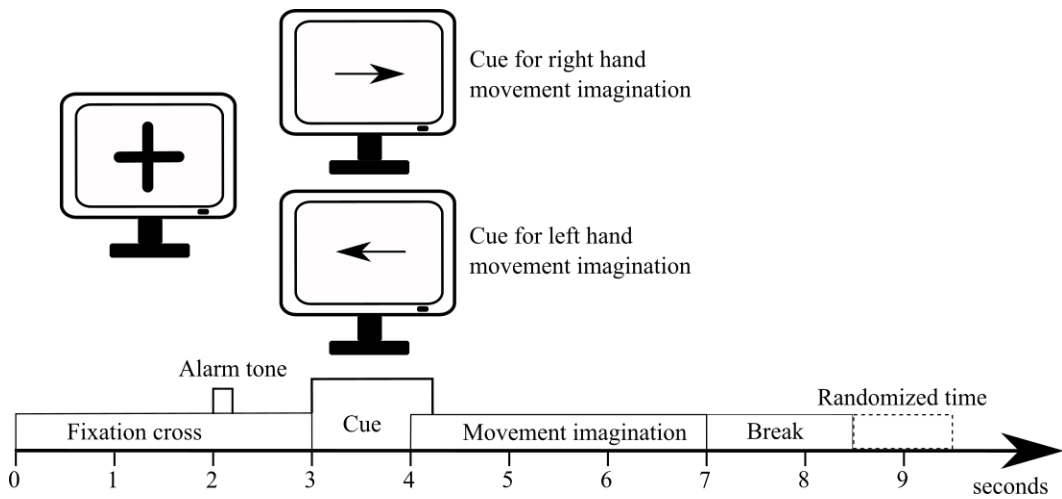


**Figure 3:** The experimental timing scheme of one trial of screening session with no feedback. Trial began with a fixation cross on screen. Then a beep sound was given to the subjects and then at second 3, the cue was presented. From second 4 till second 7, the subjects imagined the movement based on the cue presented. This figure is modified after (Leeb, et al., 2007).

In online feedback sessions with smiley feedback (see **Figure 4**), a gray smiley was centered on the screen at the start of each trial. At second 2, a short alarm beep was given to the subject. From second 3 to second 7.5, a cue was presented and based on the cue the subjects had to imagine the corresponding movement and the classifier moved the smiley towards the direction presented by the cue. The detailed description can be found in (Leeb, et al., 2007). The gray feedback smiley turned into green if it moved in the same direction as the cue, otherwise it turned into red. The screen turned black at second 7.5 which marked the end of the trial. Here, at the end of each trial a intertrial interval of 1 to 2 seconds was added.

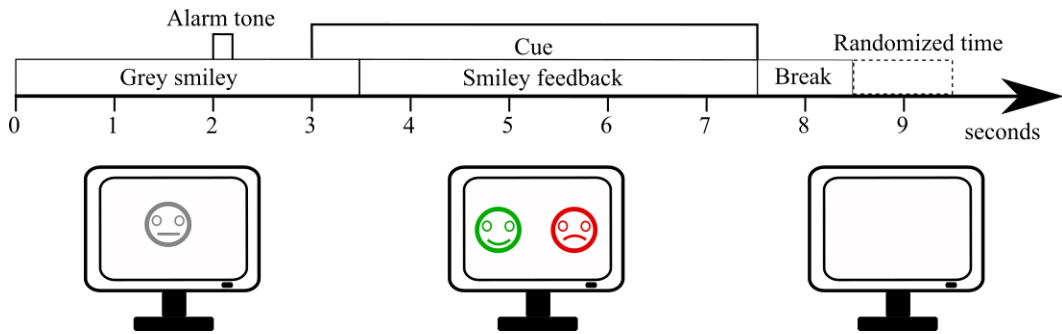


**Figure 4:** The experimental timing scheme of one trial of online feedback session with smiley. Trial began with a grey smiley at the center of the screen. Then, a beep was given to the subjects and later from second 3 till second 7.5, a cue was presented. From second 3.5 till 7.5, subjects were supposed to imagine the movement based on the presented cue and moved the smiley in the direction of cue. Smile turned green if it moved in the same direction as the cue, otherwise it turned red. This figure is modified after (Leeb, et al., 2007).

### Anchored Short-Time Fourier Transform (anchored-STFT)

Short-time Fourier transform (STFT) is a variant of Fourier transform that improves the trade-off between temporal and spectral resolution. It is used for transforming non-stationary time-series signals; signals in which the frequency components vary over time, into frequency domain. STFT

extracts the segments of the time-series signal by moving a window of fixed length on the time-series signal and applies the Fourier transform on each extracted segment of the signal, hence providing time-localized frequency information of the signal. On the contrary, the standard Fourier transform considers the entire signal and results in the frequency information that is averaged over the entire time domain and consequently loses the information about the time when these frequencies occurred in the time-series signal.

The mathematical expression of STFT as given in ([Allen & Lawrence , 1977](#)) is shown in equation (1).

$$X_m(\omega) = \sum_{n=-\infty}^{\infty} x(n) w(n - mR) e^{-j\omega n} \quad (1)$$

Where,

$x(n)$  = input signal at time  $n$ .

$w(n)$  = window function of length  $M$ .

$X_m(\omega)$  = Fast Fourier Transform of data windowed by window function  $w(n)$  centered about time  $mR$ .

$R$  = hop size/ step size (time advance in samples).

At first, a time series signal  $x(n)$  is split up into segments using a window  $w(n)$  of length  $M$ . The signal in the extracted segments is tapered based on the window function used to extract the segments. Fourier transform is applied on each extracted tapered segment of the signal and it is converted to frequency domain. Spectra of each segment of the signal is obtained which shows the strength of the frequency component with respect to time. Finally, a spectrogram is constructed by aligning the spectra of adjacent, overlapping signal segments in time-frequency plane.

Even though STFT tries to preserve the time-localized frequency information of the signal as elaborated in equation (1), yet there is still a trade-off between time and frequency resolution because of a fixed-length window that transforms the time-series signal into frequency domain. The impact of the length of the window is directly proportional to frequency resolution and inversely proportional to time resolution.

As STFT uses the fixed-length window (see **Figure 5** (a 1.1)), the frequency resolution of the STFT remains same for all the locations in the spectrogram (see **Figure 5** (a 1.2)). STFT only provides the suboptimal trade-off between time and frequency resolution. Henceforth, here an extension of STFT is proposed to address this tradeoff by defining the multiple anchors of variable lengths (see **Figure 5** (b)). The proposed algorithm is named as anchored-STFT. Anchored-STFT is inspired by wavelet transform ([DebnathJean & Antoine, 2003](#)) and Faster RCNN ([Ren S. , He, Girshick, & Sun, 2017](#)).

The working principle of anchored-STFT is as follows:

1. First, K anchors of the same shape but different lengths are defined. All the defined anchors have the same focal point (anchor position). The focal point can either be defined at the center or the left corner of the anchors (see **Figure 5 (b)** and **Figure 8**).
2. K is the maximum number of possible anchors, which is mathematically defined in equation (2)

$$K = \left\lfloor \frac{\log(sL)}{\log(2)} \right\rfloor \quad (2)$$

- $sL$  = length of the signal
- $aL^i$  = length of an anchor  $i = 2^i; i=1,2, \dots, K$
- Minimum length of an anchor =  $\min L = 2^{i=1}$
- Maximum length of an anchor =  $\max L = 2^{i=K}$
- When the focal point is defined at the centre of the anchors, then the length of the anchors is given by:  $aL^i = \text{length of an anchor } i = 2^i + 1; i=1,2, \dots, K$

3. The shape of the anchors could be selected by using the windows which are normally used by STFT e.g., Hann window etc.
4. N anchors are then selected from K using grid search method, where  $N \leq K$ .
5. The stride ‘s’ by which the anchors are slid on time-series signal is half of the length of the anchor which has the smallest length among N selected anchors in case when the focal point is defined at the left corner of the anchors. In case when the focal point is at the center of the anchors, stride ‘s’ is defined as  $(\min L_N \pm 1)/2$ .  $\min L_N$  = minimum length of the anchor among N selected anchors. Same stride is used for all N anchors. The length of the anchors and stride determine the number of anchor positions and consequently the number of segments of time-series signal that are extracted by the anchors.
6. Zero-padding is applied to the signal to ensure that the same amount of signal segments or frames are extracted for anchors of different lengths. Zero-padding is applied either on both ends of the signal or just one end depending on whether the anchors are centered around the anchor position or cornered at the anchor position.
7. Fourier transform is applied to each segment of the time-series signal extracted by anchors and converted to frequency domain (see **Figure 6**).
8. A separate spectrogram of the time-series signal is generated for each length anchor by aligning the spectra of adjacent, overlapping signal segments obtained by that length anchor as shown in **Figure 6**. For example, if anchors of 4 different lengths are used, then 4 spectra of the time-series signal are generated.
9. The overlap between anchors of the adjacent anchor locations and number of anchor locations are obtained by equation (3) and equation (4) respectively.

$$\text{overlap} = aL - \text{stride} \quad (3)$$

$$\text{no. of anchor locations} = 1 + \frac{sL - \min L_N}{s} \quad (4)$$

An illustrative representation of the time-frequency resolution of standard STFT and anchored-STFT is shown in **Figure 5** (a) and (b) respectively. A fixed length window is used in case of standard STFT, which provides suboptimal time-frequency resolution (see **Figure 5** (a)). This tradeoff is addressed by defining the anchors of different lengths (see **Figure 5** (b)). These anchors provide the resultant spectra of different time-frequency resolutions.

It is clear from **Figure 5** (a 1.2), that the frequency resolution of the STFT remains the same for all the locations in the spectrogram. However, it is shown in **Figure 5** (b 1.2) that an anchor (K1) of smaller length provides better time resolution and lower frequency resolution, whereas the anchor (K3) of longer length provides better frequency resolution and lower time resolution. The green and black boxes show the same frequency components computed for anchors of different lengths. It shows that each frequency component has different resolution for each anchor of different length which consequently provides better time-frequency resolution, which is also clearly shown in **Figure 9**. **Figure 9** shows the input images of different time-frequency resolution generated by 5 anchors of different lengths for right-hand MI-task performed by subject 4 of BCI competition IV dataset 2b.

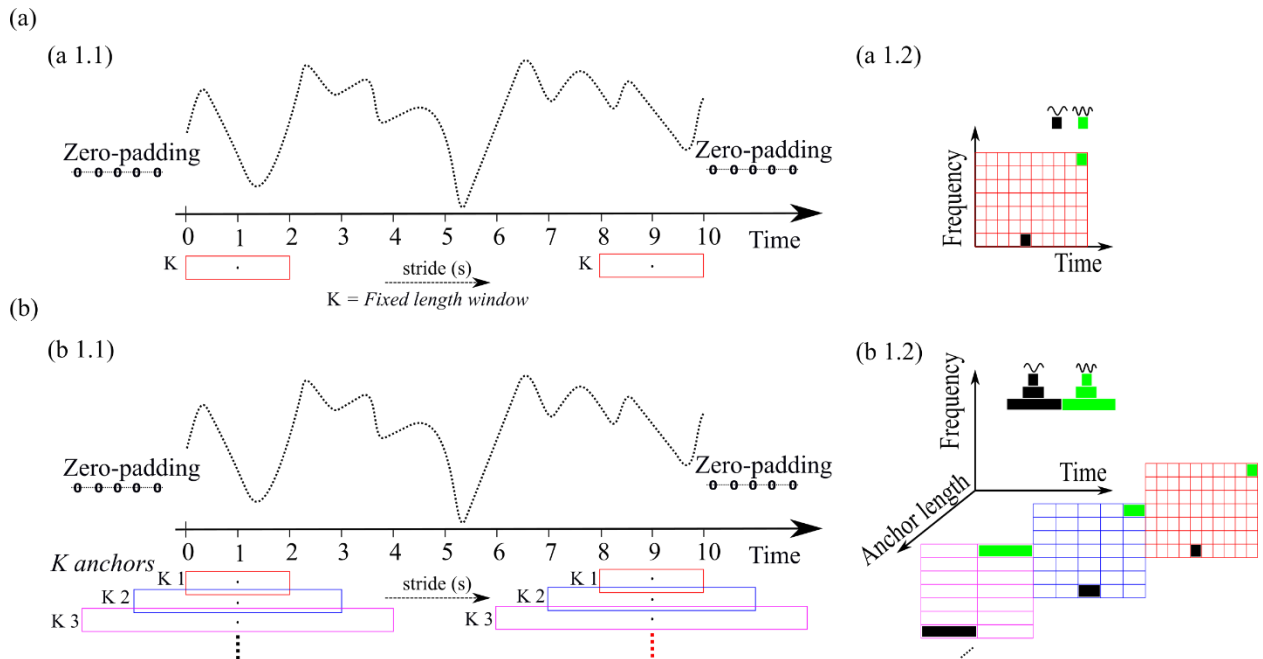


**Figure 5:** Representation of time-frequency resolution of standard STFT and anchored-STFT. (a) shows the time-frequency resolution of a fixed length window  $K$  of STFT. (a 1.1) shows a fixed length window  $K$  that is convolved with the time series signal with a fixed stride (s). (a 1.2) shows the spectrogram obtained by convolving the window  $K$  with time series signal. Here, frequency resolution remains the same for all locations of the spectrogram. (b) shows the time-frequency resolution of anchored-STFT. (b 1.1) shows that anchors of different lengths are convolved with the time series signal using stride (s). (b 1.2) shows that anchor  $K_1$  with short length results into better time resolution and low frequency resolution spectrogram. Anchor  $K_3$  with longer length provides better frequency but low time resolution spectrogram. The green and black colored boxes show a frequency component computed for anchors of different lengths which in turn provides different frequency resolution for each anchor length.

Workflow of anchored-STFT is shown in **Figure 6**. In **Figure 6**, anchors of different lengths are used to segment the time-series signal. The extracted segments of time-series signal are transformed from time domain to frequency domain. At the end, a separate spectrogram is generated for each anchor of different length. These spectra are further used by GNAA to generate augmented training data for the Skip-Net algorithm.

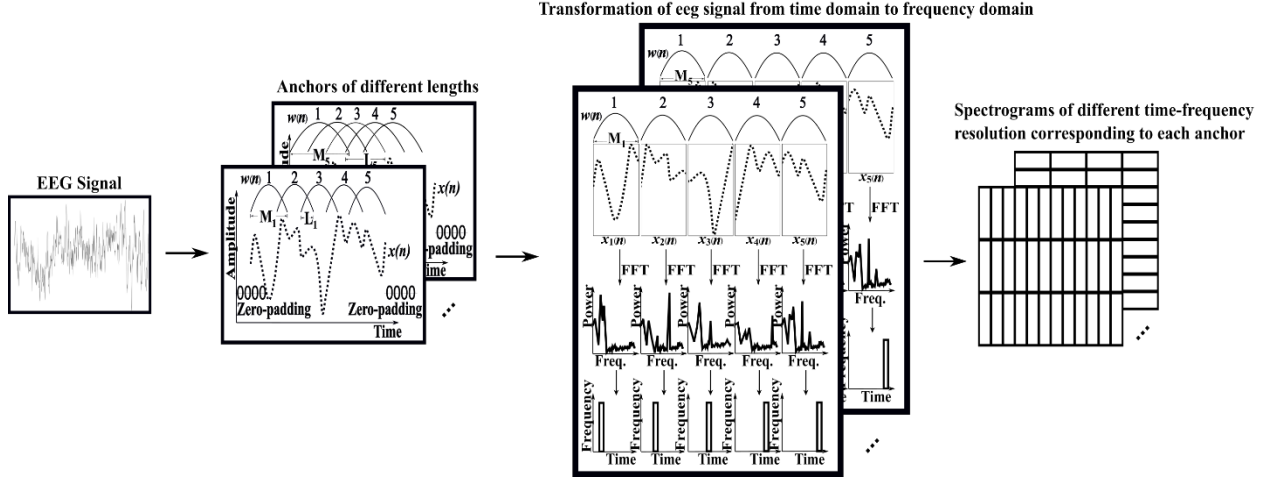


**Figure 6:** Intuitive workflow of anchored-STFT. First, the anchors of different lengths are defined which are centered around or cornered at an anchor position. The anchors are then slid along the whole signal with a constant stride. Then segments of time-series signal are extracted using those anchors. Fourier transform is applied to each segment extracted by anchors and is converted to frequency domain. A Spectrogram of different time-frequency resolution is generated for each anchor which is further used as an input image by the machine learning algorithm.

## Adversarial Data Augmentation Technique

In this study, we also propose a data augmentation technique called ‘gradient Norm (GNAA)’ for harnessing new inputs from the existing inputs for the EEG data. The proposed data augmentation algorithm is different from any other existing data augmentation techniques. At first, it requires a trained neural network for the selection of the meaningful features. Then, it calculates the gradient of cost function (of trained neural network) with respect to a given training input. This gradient provides the direction of the decision boundary. The given training input  $x$  is slightly perturbed (by factor  $\epsilon$ ) towards the direction of decision boundary. As a result, it generates new inputs  $x_{new}$  as shown in equation (5). ‘Gradient norm’ method is not only a method of generating new inputs, but it also ensures the selection of features in the given feature vector that play a pivotal role in the prediction.

$$x_{new} = x + \epsilon \left( \frac{\frac{\partial(\text{cost})}{\partial x}}{\left| \frac{\partial(\text{cost})}{\partial x} \right|} \right) \quad (5)$$

We not only used equation (5) for data generation but also to study the existence of adversarial inputs in the domain of BCI studies. In this study, we define the term ‘adversarial inputs’ as the

inputs which are modified versions of original inputs but are highly correlated, however the employed classification algorithm fails to predict them correctly. Here, the term  $\beta$  in the equation (6) defines the required minimum amount of perturbation, such that, the difference between two inputs (original input and perturbed input) remains indistinguishable in terms of correlation but the classifier can be fooled with perturbed inputs. The value of  $\beta$  is (0.01) determined empirically.

$$x_{adv} = x + \beta \left( \frac{\frac{\partial(cost)}{\partial x}}{\left| \frac{\partial(cost)}{\partial x} \right|} \right) \quad (6)$$

Here, we also determine the ‘pockets’ of adversarial inputs. The ‘pockets’ are defined as the number of inputs in the train dataset that can be converted into adversarial inputs (using trained classifier) by applying the amount of perturbation defined by  $\beta$  in equation (6).

Additionally, we compared the perturbation applied by the ‘gradient norm’ method with another existing method of crafting adversarial inputs called ‘gradient sign’ method (Goodfellow, Shlens, & Szegedy, 2014) defined in equation (7). The perturbation applied by the two methods are significantly different as shown in **Figure 7**. The perturbation applied by the gradient norm method is shown in **Figure 7** (a) and the perturbation applied by the gradient signum method is shown in **Figure 7** (b). The perturbation applied by the ‘gradient norm’ method carefully selects only features that are important for the employed classification algorithm as shown in **Figure 7** (a). However, the perturbation applied by the ‘gradient sign’ method seems to be random (see **Figure 7**(b)). The randomness lies in the perturbation because of the signum operator in equation (7). The signum operator maps all the values greater than zero to 1 and the values less than zero to -1 in the perturbation matrix (see **Figure 7** (b)). Mathematically, the signum operator is defined in equation 8. As a result, the perturbation matrix is filled with values of either 1 or -1 and importance of each feature is disregarded.

$$x_{adv} = x + \varepsilon \operatorname{sign} \left( \frac{\partial(cost)}{\partial x} \right) \quad (7)$$

$$\operatorname{sign} := \begin{cases} -1 & \text{if } x < 0 \\ 0 & \text{if } x = 0 \\ 1 & \text{if } x > 0 \end{cases} \quad (8)$$

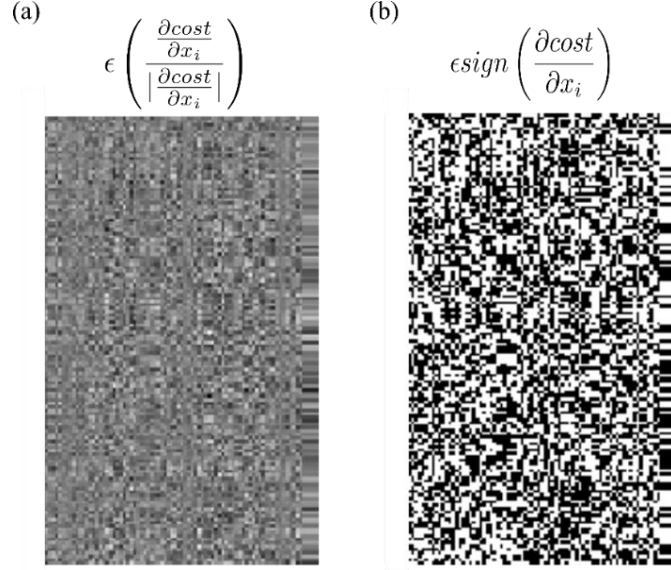


**Figure 7:** Comparison of perturbations offered by two methods; gradient norm method and gradient signum method. (a) On the left-hand side, the perturbations produced by gradient norm are shown. (b) on the right-hand side, the perturbations produced by gradient signum method are shown.

In this study, we presented a comprehensive analysis of adversarial inputs using the method presented in equation (5) and used the same method to generate new training inputs from the existing inputs. During the generation of new inputs, we only consider those inputs which were not converted to adversarial inputs using equation (6).

## Feature formation

In this study we used a convolutional neural network (CNN) based algorithm called Skip-Net for the classification of MI-EEG signals. Since the CNN based algorithms have shown state-of-art results in image recognition, therefore we also converted the EEG signals into images to use for classification by the Skip-Net algorithm.

In case of BCI competition IV dataset 2b, the EEG signal from second 3 to second 5.5 (2.5 seconds in total) is considered for each trial and converted into frequency domain using anchored-STFT (see section 2.2). We call this interval (from second 3 to second 5.5) of the EEG signal the signal of interest (SOI) in the rest of the document. The SOI for dataset III BCI competition II lasts from second 2.75 to second 7.25. In case of 250 Hz sampling frequency, each SOI consists of 625 samples. Anchors of five different lengths are used to transform each SOI into frequency domain. So, we get five spectrums of different time-frequency resolution for each SOI. We treat these spectra as images. The lengths (in samples) of anchors used are as follows: 16, 32, 64, 128, 256. All the lengths considered are of power of 2. Stride of 8 samples is used to slide each anchor across the SOI. Here the anchors are cornered at the anchor positions as shown in **Figure 8**. Anchor with the shortest length (8 samples) and the stride are used to determine the number of anchor positions (see equation (1)) for all the anchors and consequently the number of segments into which each SOI is divided. This results in 78 anchor locations or segments for an SOI. Since the first anchor position considered is the first sample of the SOI, so the zero-padding is only applied after the last sample of the SOI such that the 78 segments are extracted from SOI for each anchor. Equation (8)

is used to calculate the zero-padding required. 257 unique FFT points as used by (Tabar & Halici, 2017) are used to get the frequency components. This leads to a  $257 \times 78$  image (spectrum) for each anchor, where 257 and 78 are the number of samples along the frequency and time axes, respectively.

$$\text{Zero}_{\text{padding}} = \text{stride} * (\text{no. of anchor locations} - 1) - \text{signal length} + \text{anchor length} \quad (8)$$

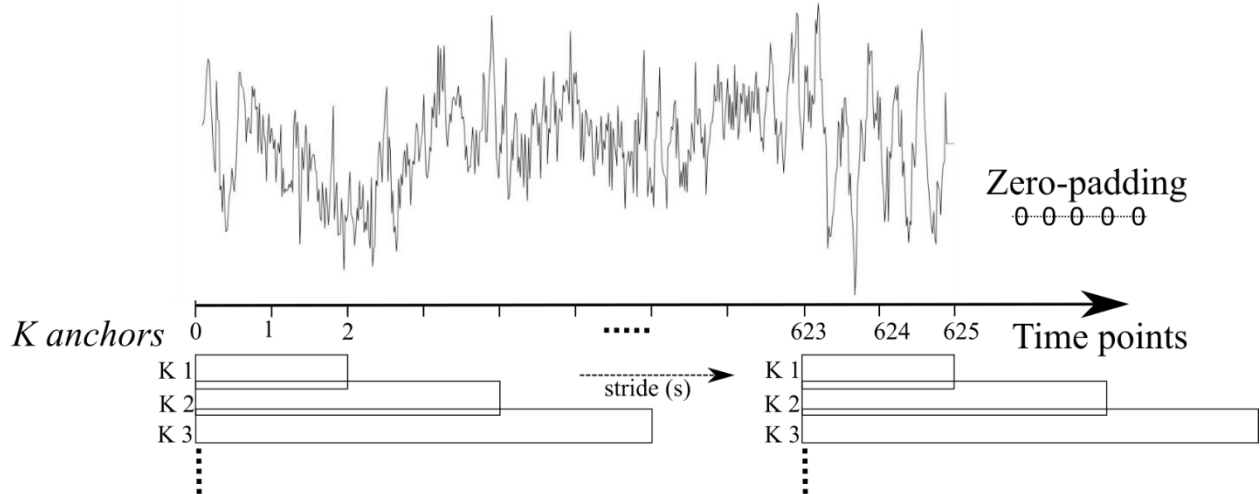


**Figure 8:** SOI of one right hand MI-task. The anchors are cornered at the anchor positions and zero-padding is applied after the last sample of the SOI to extract the equal number of segments for all the anchors for the SOI.

(Pfurtscheller & FH Lopes Da Silva, 1999) has shown that mu band (8-13 Hz) and beta band (13-30 Hz) are of high interest for the classification of MI-EEG signals. Since there is an event related desynchronization (ERD) and event related synchronization (ERS) in mu and beta bands respectively when an MI task is performed, therefore these bands are very vital for the classification of MI-EEG signals. So, we just considered these bands for further processing. The mu band is represented by frequencies between 4-15 Hz and beta band is represented by the frequencies between 19-30 Hz. We then extracted the mu and beta frequency bands from each spectrum of a SOI. The size of images for extracted mu and beta frequency bands is  $22 \times 78$  and  $23 \times 78$ , respectively. To get the equal representation of each band, we resized the beta band to  $22 \times 78$  using cubic interpolation method. Finally, we combined these images to get an image of size  $N_{fr} \times N_t$  ( $44 \times 78$ ); where  $N_{fr} = 44$  (no. of frequency components) and  $N_t = 78$  (no. of time sample points). Since, the dataset contains the EEG signals from  $N_c = 3$  electrodes ( $C_3$ ,  $C_z$  and  $C_4$ ), we repeat the same process for all three electrodes and combine all these images from three electrodes which results in a final image of size  $N_h \times N_t$  ( $132 \times 78$ ); where  $N_h = N_{fr} \times N_c = 132$  for one anchor. We then repeat the whole process for all five anchors and get 5 images of size  $132 \times 78$  each for each SOI. **Figure 9** shows the input images generated by using 5 anchors for an SOI of right-hand MI-task performed by subject 4.

The decrease of energy in mu band (4 -15 Hz) and increase of energy in beta band (19 - 30Hz) in the C3 channel clearly shows the ERD and ERS effect respectively for this right-hand MI-task, which is common while performing a MI-task.

Same process is done for dataset III of BCI competition II to get the input features.

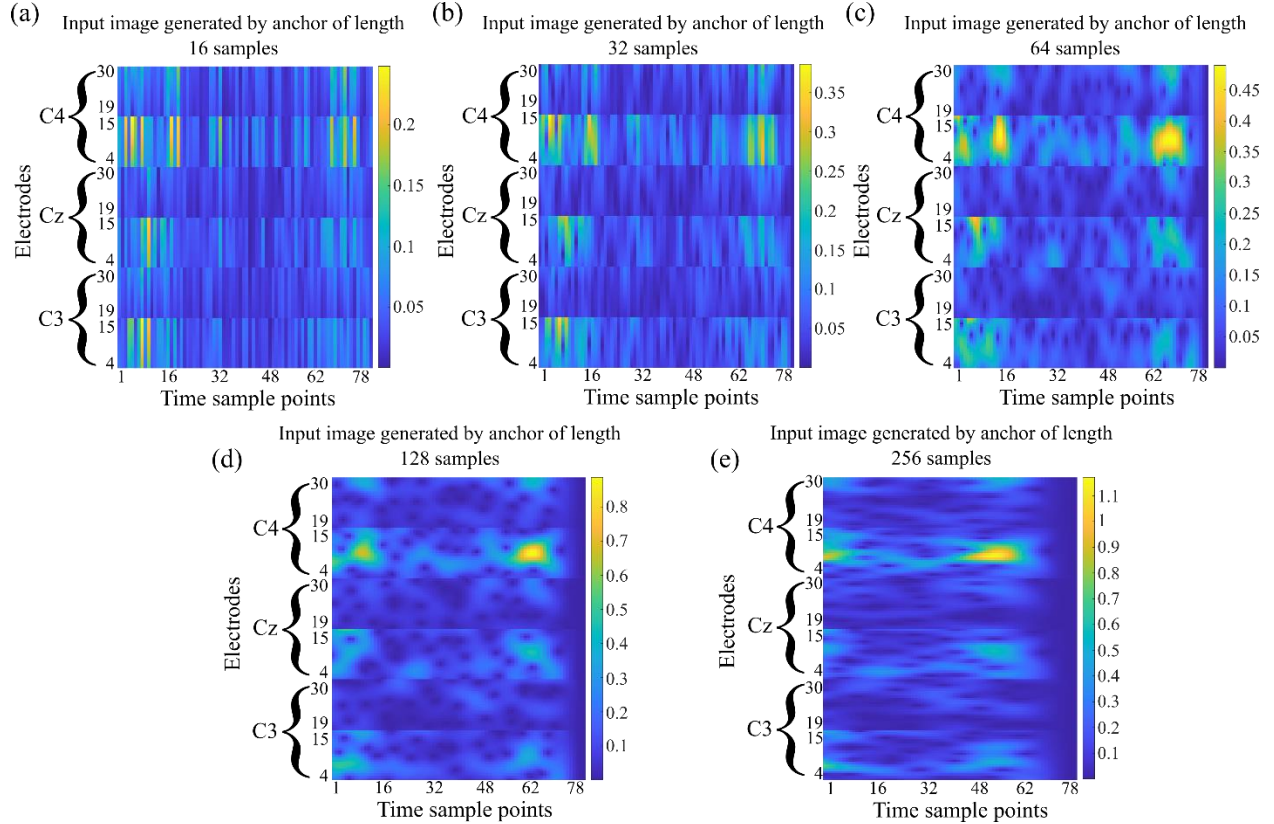


**Figure 9:** Input images generated by 5 anchors from an SOI of right-hand MI-task performed by subject 4.

### Skip-Net

In this study, we proposed a novel architecture for the classification of MI-EEG signals which contains one skip connection, hence named as Skip-Net. The architecture of the Skip-Net is shown in **Figure 10**. First layer in Skip-Net architecture is the input layer. The dimensions of the input layer are  $N_h \times N_t$ . The second layer is the convolutional layer which uses 16 kernels of size  $N_h \times 1$  to convolve the input image at a stride of 1 in both horizontal and vertical directions. Rectified linear units (ReLUs) are used as the activation functions.

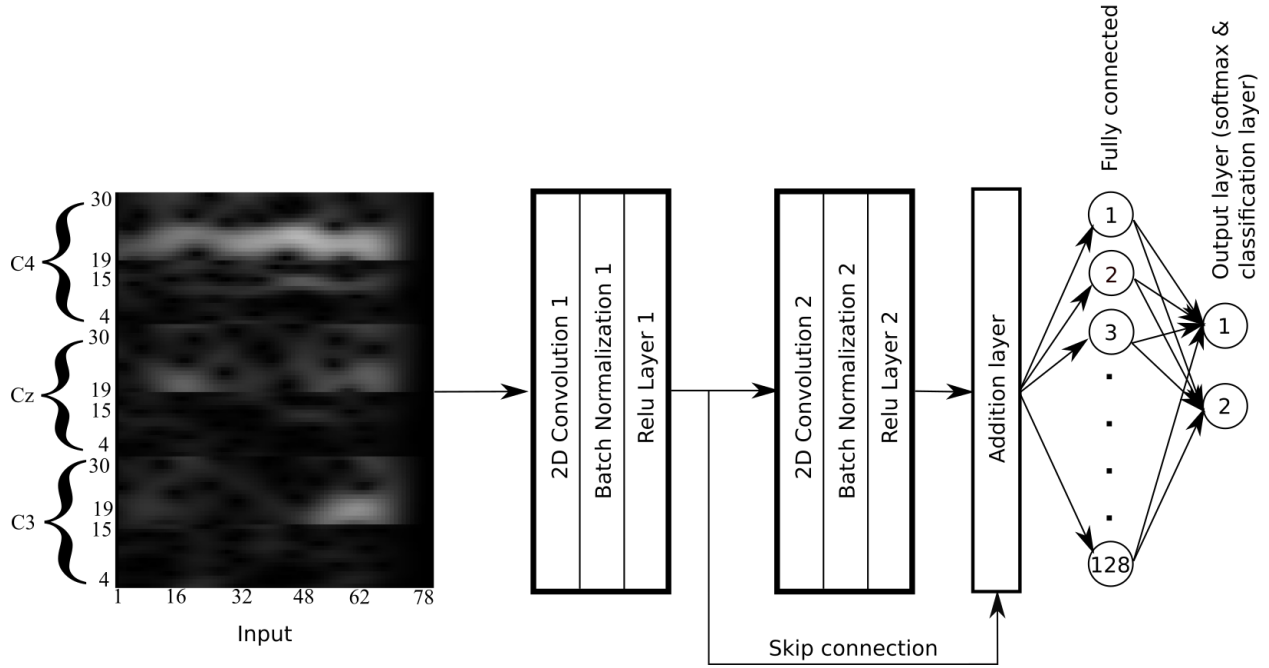


**Figure 10:** Illustration of the Skip-Net architecture for the classification of MI-EEG signals.

The output of the convolutional layer is of the size  $1 \times N_t \times 16$ . Batch normalization is applied at the output of the convolutional layer. The next layer is the second convolutional layer which uses 16 kernels of size  $1 \times 3$  to convolve the output of the last layer in horizontal direction with a stride of 1. ReLUs are used here as the activation function and batch normalization is also applied at the output of the second convolutional layer. Next layer is the addition layer which adds the output of the first ReLU and second ReLU function. Same padding is applied in the second convolutional layer to keep the dimensions of the second convolutional feature map to be the same as the output of the first convolutional feature map so that both feature maps are compatible for the addition layer. The output of the addition layer is then fed to a fully connected layer which has 128 neurons and uses a dropout of 50 % as regularization to avoid overfitting. ReLUs are also used as activation function here. The last layer is the output layer which uses Softmax function to output the predictions.

## Training

The hyperparameters and their corresponding values after tuning used to train the Skip-Net algorithm are shown in **Table 1**.

**Table 1:** Training parameters that are used for the training of the Skip-Net algorithm.

S. No	Parameter	Value
1	Optimization algorithm	Stochastic gradient descent with momentum (SGDM)
2	Momentum	0.9
3	Initial Learning rate	0.01

4	Learning rate drop factor	0.5
5	Learning rate drop period	5 epochs
6	Regularization	L2 norm (0.01), Dropout (0.5)
7	Max Epochs	100
8	Mini batch size	200

## Evaluation

It is shown in **Figure 1** that the features (spectra) generated by anchored-STFT are directly used by the Skip-Net algorithm to produce the classification results in test mode. As mentioned in section **Feature formation** that each SOI is transformed into 5 spectra of different time-frequency resolutions, Skip-Net classifies each spectrogram into one class which results in 5 predicted outputs for each SOI (one for each spectrogram). Final classification is based on majority voting using the 5 predicted outputs. The reliability tag is given based on the number of occurrences of the final classification class. The number of anchors (N) used must be odd to prevent ties. We define a reliability tag greater than 0.6 as ‘reliable’ and a reliability tag is less than or equal to 0.6 as ‘partially reliable’. The threshold for the reliability tag is a hyperparameter that can be freely chosen. Here we chose a value of 0.6 which means at least four out of five predictions must correspond to the correct class. The graphical representation of the forward pass of the whole pipeline during the testing mode is shown in **Figure 11**.

**We would upload the code and the trained models on GitHub after the successful publication of the manuscript so that others could also use it.**

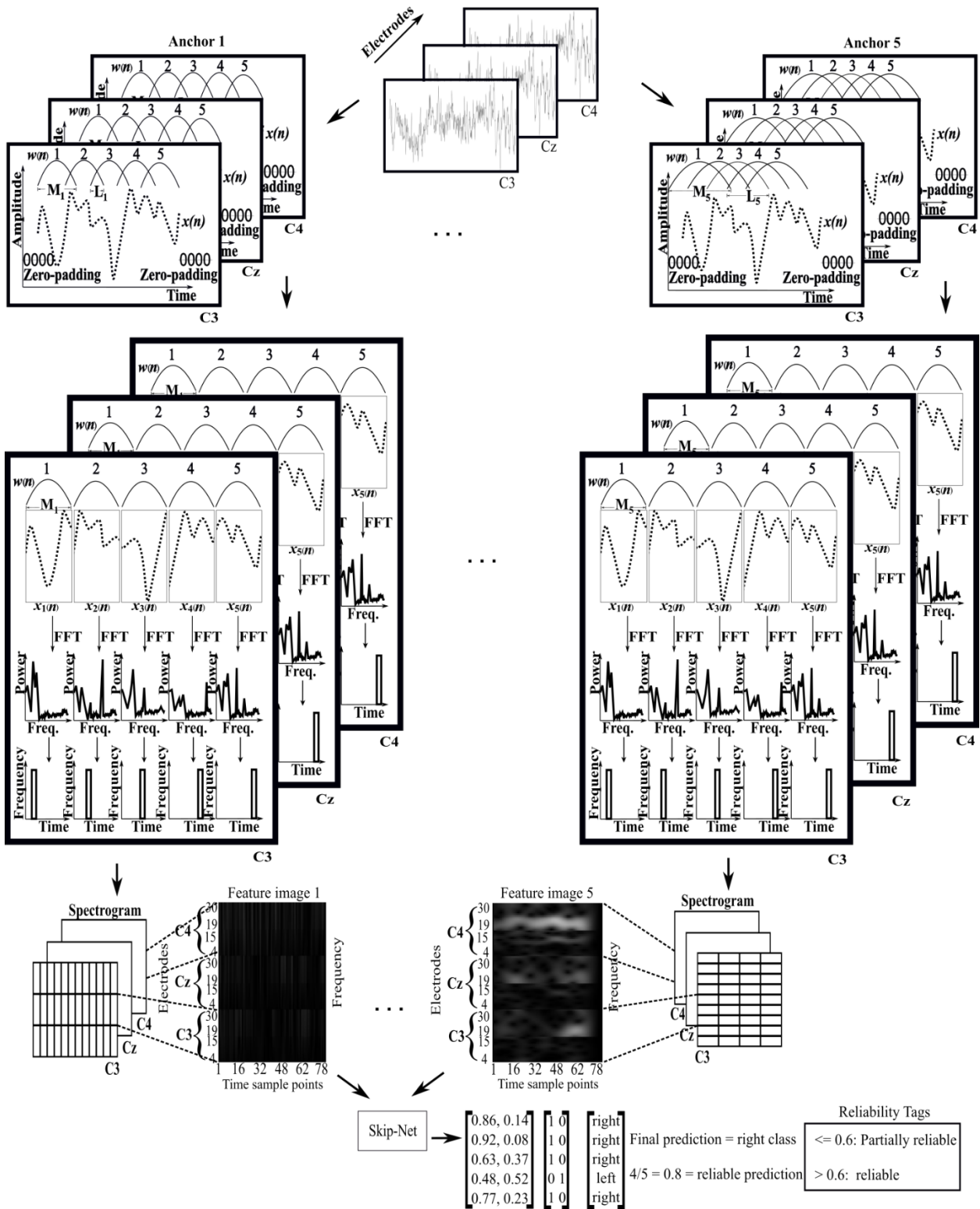


**Figure 11:** Graphical representation of whole pipeline in testing mode. Five spectra are computed for each SOI for each channel. Each spectrogram is then fed to Skip-Net to make five predictions in total for each SOI. Voting is done on five output predictions. Class with maximum number of occurrences is the final predicted class for an SOI. The reliability tag of the final prediction is calculated by the number of occurrences of the final predicted class divided by 5. Reliability tag  $> 0.6$  means reliable prediction and  $\leq 0.6$  means partially reliable prediction.

# Results

Here, we present the comparison of the proposed pipeline with the different existing algorithms presented in (Tabar & Halici, 2017), (Keng Ang, Yang Chin, Wang, Guan, & Zhang, 2012), (Suk & Seong-Whan, 2011), (Gandhi, et al., 2011), (Shahid, Sinha, & Prasad, 2010) and (Lemm, Schäfer, & Curio, 2004). Few of the aforementioned studies used the publicly available dataset III from BCI competition II and the remaining used dataset 2b from BCI competition IV. Only one of aforementioned studies used both datasets (Tabar & Halici, 2017). These datasets are considered as benchmarks for EEG based BCI decoding applications. We also used both datasets for comparison.

Dataset III from BCI competition II contains the EEG-MI data of 1 subject. This dataset was recorded from three electrodes (C3, Cz and C4) placed over the motor cortex areas of the brain. BCI competition IV dataset 2b contains the EEG-MI data of 9 subjects which was also recorded from three electrodes (C3, Cz and C4) placed over the motor cortex areas of the brain.

## Evaluation metrics

We used the accuracy and kappa values as the metrics to compare the classification results of our proposed method and the current existing studies. The kappa value shows the classification performance by removing the effect of accuracy of random classification. Kappa value is calculated by equation (9).

$$\kappa = \frac{\text{accuracy} - \text{random accuracy}}{1 - \text{random accuracy}} \quad (9)$$

In equation (9), the accuracy is the predicted classification accuracy, and the random accuracy is 0.5 in case of two class classification task.

## Performance comparison of the proposed pipeline with existing algorithms on different publicly available datasets

### Session-to-session classification performance (BCI competition IV dataset 2b)

We performed two experiments for BCI competition IV dataset 2b. In the first experiment, we evaluated the session-to-session classification performance of our proposed pipeline and compared the performance with existing algorithms. We compared our proposed feature extraction and classification algorithm with two existing feature extraction and classification methods proposed in (Tabar & Halici, 2017) and (Ang et al, 2012).

### Session-to-session classification performance in comparison with (Tabar & Halici, 2017)

(Tabar & Halici, 2017) used STFT for feature vector extraction and employed deep-learning architectures for classification which includes CNN, stacked autoencoder (SAE) and CNN in conjunction with stacked autoencoder (CNN-SAE). Here, they used the first two training sessions (01T and 02T) for training the algorithms and the remaining third session (03T) for evaluation. They used accuracy results as the performance metrics. Henceforth, we also used the same data for training and evaluation and same performance metric for comparison of our proposed pipeline in this analysis.

**Table 2** shows the comparison of the evaluation accuracy of the proposed method (anchored-STFT + Skip-Net with/without GNAA) with CNN, SAE, and CNN-SAE methods in session-to-session classification task. Here, it is shown that anchored-STFT + Skip-Net with GNAA yielded the highest average accuracy value of 78.0 % compared to the other methods. It indicates that our method with GNAA provided 2.9 % higher average accuracy with respect to CNN-SAE method, whereas it provided 5.6 % and 7.7 % improvement in average accuracy with respect to CNN and SAE methods, respectively. Anchored-STFT + Skip-Net without GNAA improved the average accuracy by 1.8 %, 4.5 % and 6.6 %, when compared with CNN-SAE, CNN, and SAE, respectively.

**Table 2** shows that, anchored-STFT + Skip-Net with GNAA outperformed CNN-SAE, CNN and, SAE for 6 out of 9 subjects whereas, anchored-STFT + Skip-Net alone outperformed CNN-SAE, CNN and, SAE for 5 out of 9 subjects.

**Table 2:** Comparison of accuracy results generated by CNN, SAE, CNN-SAE ([Tabar & Halici, 2017](#)) and anchored-STFT + Skip-Net with/without GNAA for session-to-session classification task (trained on 01T and 02T sessions and evaluated on 03T session) of dataset 2b from BCI competition IV.

Subjects	CNN	SAE	CNN-SAE	anchored-STFT + Skip-Net	anchored-STFT + Skip-Net with GNAA (epsilon = 0.01)
S1	76.3	57.5	78.1	76.0	76.9
S2	60.0	58.1	63.1	54.2	55.6
S3	56.3	50.6	60.6	53.5	54.4
S4	95.6	94.4	95.6	<b>95.9</b>	<b>97.5</b>
S5	79.4	75.0	78.1	<b>87.9</b>	<b>88.8</b>
S6	65.6	67.5	73.8	73.2	<b>74.4</b>
S7	65.6	76.2	70.0	<b>80.6</b>	<b>81.9</b>
S8	70.6	75.6	71.3	<b>85.0</b>	<b>85.6</b>
S9	82.5	78.1	85.0	<b>86.2</b>	<b>86.9</b>
Average	72.4	70.3	75.1	<b>76.9</b>	<b>78.0</b>

### Session-to-session classification performance in comparison with ([Ang et al, 2012](#))

In ([Ang et al, 2012](#)), Filter Bank Common Spatial Pattern (FBCSP) algorithm is used for feature vector extraction and classification. FBCSP is also the winner algorithm of BCI competition IV dataset 2b as reported in ([Ang et al, 2012](#)). In addition to FBCSP, a performance comparison with common spatial pattern (CSP) algorithm is also presented. Here, they used all the three training sessions (01T, 02T and 03T) for training and the evaluation sessions (04E and 05E) for testing their algorithm in session-to-session classification analysis. They used kappa value results as performance metrics. Kappa value can be calculated using the equation (9). We also used the same data for training and evaluation and the same performance metrics to compare the performance of our algorithm with FBCSP and CSP methods in this analysis.

**Table 3** shows the kappa value results of the proposed method (anchored-STFT + Skip-Net with/without GNAA) and its comparison with common spatial pattern (CSP) and FBCSP

algorithms in session-to-session classification task. Here, it is shown that anchored-STFT + Skip-Net with GNAA yielded the highest average kappa value of 0.618 compared to the other methods. It indicates that our method with GNAA provided 18.8 % and 3.2 % improvement in terms of average kappa value with respect to CSP and FBCSP methods, respectively. In case of anchored-STFT + Skip-Net without GNAA, these numbers are 18.3 % and 2.7 % respectively.

**Table 3** shows that, our method (anchored-STFT + Skip-Net with / without GNAA) outperformed FBCSP algorithm for 5 out of 9 subjects whereas, it outperformed CSP algorithm for 8 out of 9 subjects.

**Table 3:** Comparison of Kappa results generated by CSP, FBCSP (Keng Ang, Yang Chin, Wang, Guan, & Zhang, 2012) and anchored-STFT + Skip-Net with/without GNAA for session-to-session classification task (trained on 01T, 02T and 03T sessions and evaluated on 04E and 05E sessions) of dataset 2b from BCI competition IV.

Subjects	CSP	FBCSP	anchored-STFT + Skip-Net	anchored-STFT + Skip-Net (GNAA)
S1	0.319	0.400	<b>0.500</b>	<b>0.494</b>
S2	0.229	<b>0.207</b>	0.100	0.100
S3	0.125	<b>0.219</b>	0.162	0.182
S4	0.925	<b>0.950</b>	0.938	0.938
S5	0.525	<b>0.856</b>	0.850	0.844
S6	0.500	0.613	<b>0.738</b>	<b>0.744</b>
S7	0.544	0.550	<b>0.626</b>	<b>0.638</b>
S8	0.856	0.850	<b>0.868</b>	<b>0.868</b>
S9	0.656	0.744	<b>0.750</b>	<b>0.756</b>
Average	0.520	0.599	<b>0.615</b>	<b>0.618</b>

### Single trial classification performance (BCI competition IV dataset 2b)

In addition to session-to-session classification task, we also evaluated the single trial classification performance of our proposed pipeline using 10 x 10-fold cross-validation on training dataset and compared the performance with the winner algorithm (FBCSP) of the competition. In each session 90 % of the training trails without artifacts were selected randomly for training and the remaining 10 % were used for testing. **Table 4** shows the evaluation performance of the proposed method (anchored-STFT + Skip-Net with/without GNAA) and FBCSP algorithm in terms of kappa values. During cross validation, the data augmentation technique (GNAA) is used to enhance the training data of each fold where anchored-STFT + Skip-Net in conjunction with GNAA is used. However, in case of FBCSP and anchored-STFT + Skip-Net without GNAA, no data augmentation is applied on training data.

Here, the average kappa value of the FBCSP (which is the winner algorithm of the BCI competition IV dataset 2b) method is 0.502, whereas the anchored-STFT + Skip-Net with / without GNAA obtained the average kappa value of 0.520 and 0.505, respectively. The higher kappa value of the proposed methods in comparison with the FBCSP method indicates the high generalization quality.

The proposed pipeline (with / without GNAA) increased the kappa value by 3.6 % and 0.59 %, respectively with respect to FBCSP.

**Table 4** shows that the proposed approach with / without GNAA outperformed FBCSP method for 6 out of 9 subjects.

**Table 4:** Comparison of Kappa results generated by FBCSP (Keng Ang, Yang Chin, Wang, Guan, & Zhang, 2012) and anchored-STFT + Skip-Net with/without GNAA for single trial classification task of dataset 2b from BCI competition IV.

Subjects	FBCSP	anchored-STFT + Skip-Net	anchored-STFT + Skip-Net (GNAA)
S1	$0.546 \pm 0.017$	<b><math>0.574 \pm 0.104</math></b>	<b><math>0.598 \pm 0.074</math></b>
S2	<b><math>0.208 \pm 0.028</math></b>	$0.146 \pm 0.159$	$0.145 \pm 0.142$
S3	<b><math>0.244 \pm 0.023</math></b>	$0.116 \pm 0.171$	$0.124 \pm 0.163$
S4	$0.888 \pm 0.003$	<b><math>0.900 \pm 0.052</math></b>	<b><math>0.902 \pm 0.047</math></b>
S5	$0.692 \pm 0.005$	<b><math>0.722 \pm 0.059</math></b>	<b><math>0.749 \pm 0.055</math></b>
S6	$0.534 \pm 0.012$	<b><math>0.649 \pm 0.095</math></b>	<b><math>0.662 \pm 0.082</math></b>
S7	$0.409 \pm 0.013$	<b><math>0.444 \pm 0.102</math></b>	<b><math>0.512 \pm 0.060</math></b>
S8	$0.413 \pm 0.013$	<b><math>0.452 \pm 0.069</math></b>	<b><math>0.427 \pm 0.068</math></b>
S9	<b><math>0.583 \pm 0.010</math></b>	$0.542 \pm 0.090$	$0.558 \pm 0.073$
Average	$0.502 \pm 0.014$	<b><math>0.505 \pm 0.100</math></b>	<b><math>0.520 \pm 0.092</math></b>

### Maximum Kappa value comparison

In addition to average kappa values for 10 x 10-fold cross validation, we also compared the performance of anchored-STFT + Skip-Net with GNAA with some other methods that provided the best kappa values only for dataset 2b of BCI competition IV. We used the best kappa values of anchored-STFT + Skip-Net with GNAA for this comparison as shown in **Table 5**. It is shown in **Table 5** that the average of the best kappa value of our method is higher than all the other methods. Our method outperformed DDFBS (Suk & Seong-Whan, 2011) and Bi-Spectrum (Shahid, Sinha, & Prasad, 2010) for 6 out of 9 subjects, whereas it outperformed CNN-SAE for 5 out of 9 subjects, whereas it outperformed and RQNN (Gandhi, et al., 2011) for 4 out of 9 subjects.

**Table 5:** Comparison of best kappa values of anchored-STFT + Skip-Net with GNAA, CNN-SAE (Tabar & Halici, 2017), DDFBS (Suk & Seong-Whan, 2011), Bi-Spectrum (Shahid, Sinha, & Prasad, 2010) and RQNN (Gandhi, et al., 2011).

Subjects	Best kappa value without subjects 2 and 3				
	CNN-SAE	DDFBS	Bi-Spectrum	RQNN	anchored-STFT + Skip-Net (GNAA)
S1	0.738	0.710	0.600	0.640	<b>0.758</b>
S2	0.458	0.310	0.310	<b>0.590</b>	0.442
S3	<b>0.845</b>	0.750	0.300	0.650	0.640
S4	<b>1.000</b>	0.470	0.980	0.990	0.950
S5	0.750	0.190	0.660	0.460	<b>0.900</b>
S6	0.796	0.200	0.610	0.510	<b>0.820</b>
S7	0.699	0.780	0.750	<b>0.810</b>	0.722
S8	0.751	0.770	<b>0.800</b>	<b>0.800</b>	0.576
S9	0.550	0.730	0.760	0.770	<b>0.832</b>
Average	0.732	0.546	0.641	0.691	<b>0.737</b>

### Classification performance on BCI competition II dataset III

To further validate the performance of our method, we employed our proposed pipeline on another publicly available dataset III from BCI competition II. Since this dataset is well divided into training and test data, the evaluation of the presented pipeline is trivial. Here, we only performed the evaluation on the unseen (test) dataset. We computed the input images as explained in the section **Feature formation**. **Table 6** shows the comparison of classification accuracy and kappa values on this dataset produced by anchored-STFT + Skip-Net (with / without GNAA), CNN, CNN-SAE, and the winner algorithm (Lemm, Schäfer, & Curio, 2004) of the BCI competition II on dataset III.

**Table 6:** Comparison of accuracy and kappa results on BCI competition II dataset III produced by anchored-STFT + Skip-Net (with/without GNAA), CNN, CNN-SAE (Tabar & Halici, 2017) and the winner algorithm (Lemm, Schäfer, & Curio, 2004).

	CNN	CNN-SAE	winner algorithm	anchored-STFT	anchored-STFT+Skip-Net (GNAA)
Accuracy	89.3	90.0	89.3	<b>90.7</b>	<b>90.7</b>
Kappa	0.786	0.800	0.783	<b>0.814</b>	<b>0.814</b>

**Table 6** shows that our method (with / without GNAA) outperformed the winner algorithm and provided 1.4 % and 3.9 % improvement in terms of accuracy and kappa value, respectively. It also outperformed CNN and CNN-SAE methods by 1.4 % and 0.7 %, respectively in terms of accuracy and 3.56 % and 1.75 %, respectively in terms of kappa values.

### Reliability tags of session-to-session classification task on both datasets

Here, we present the percentage of the reliability tags generated by anchored-STFT + Skip-Net in conjunction with GNAA on both datasets for the session-to-session classification task. The reliability tag as shown in **Figure 11** is the ratio of the total count of occurrences of final predicted class over the total predictions made per trial. Its value ranges from 0 to 1. Reliability tag of greater

than 0.6 is labeled as reliable prediction, whereas a value equal or less than 0.6 is labeled as partially reliable prediction (see Evaluation section). Total predictions made per trial depend on the number of used anchors (N). **Table 7** shows the percentage of the reliable and partially reliable predictions out of all the final predictions made on each subject of both datasets. It also shows the percentage of correct predictions out of reliable predictions for each subject.

**Table 7:** Reliability tags of predicted results by anchored-STFT + Skip-Net in conjunction with GNAA on both datasets.

anchored-STFT + Skip-Net (GNAA)										
Datasets	BCI comp. IV dataset 2b								BCI comp. II dataset III	
Subjects	S1	S2	S3	S4	S5	S6	S7	S8	S9	
Reliable (%) (Correct Pred. %)	77.8 (77.5)	55.7 (56.4)	61.9 (63.1)	98.1 (96.8)	88.4 (96.5)	81.0 (92.6)	82.2 (84.4)	92.0 (96.3)	92.0 (90.1)	91.0 (92.2)
Partially reliable (%)	22.2	44.3	38.1	1.9	11.6	19.0	17.8	8.0	8.0	9.0
Average (%)	Reliable (R) = 81.01      Partially reliable (PR) = 18.98								R = 91.0 PR = 9.0	

It can be seen from **Table 7**, that for BCI competition IV, dataset 2b, 81.01 % of all predictions of our proposed method were considered reliable and 18.98 % were partially reliable predictions. In case of BCI competition II, dataset III, these numbers were 91 % and 9 % respectively.

### Adversarial Augmentation

We showed that the proposed data augmentation technique helps to improve the classification accuracy and kappa values as shown in **Table 2**, **Table 3**, and **Table 4**. Additionally, it increases the robustness of the classification algorithm by reducing the standard deviation as shown in **Table 4**.

In this analysis, the visualization of the perturbations offered by two methods are shown in **Figure 12 & Figure 13**. **Figure 12** shows the original input (correctly classified) (**Figure 12 (a)**), the perturbation generated by the gradient norm method (**Figure 12 (b)**), and the synthetic input generated (**Figure 12 (c)**) by adding the perturbation introduced by the gradient norm method into the original input. Similarly, **Figure 13** represents the impact of different kinds of perturbations generated using the gradient sign method (Goodfellow, Shlens, & Szegedy, 2014).

The perturbations generated by gradient norm method are shown in **Figure 12 (b)** and the perturbations generated by gradient sign method are shown **Figure 13 (b)**. These figures show that the introduced perturbations are quite different. The gradient norm method (see **Figure 12 (b)**) changes the value of each element (feature) of the matrix with different values. Here, the change of the feature value depends on its importance for the classification algorithm. The more important

features are replaced with higher values and the value of the least important feature is slightly changed. The direction of the perturbations tends to be towards the decision boundary for both methods.

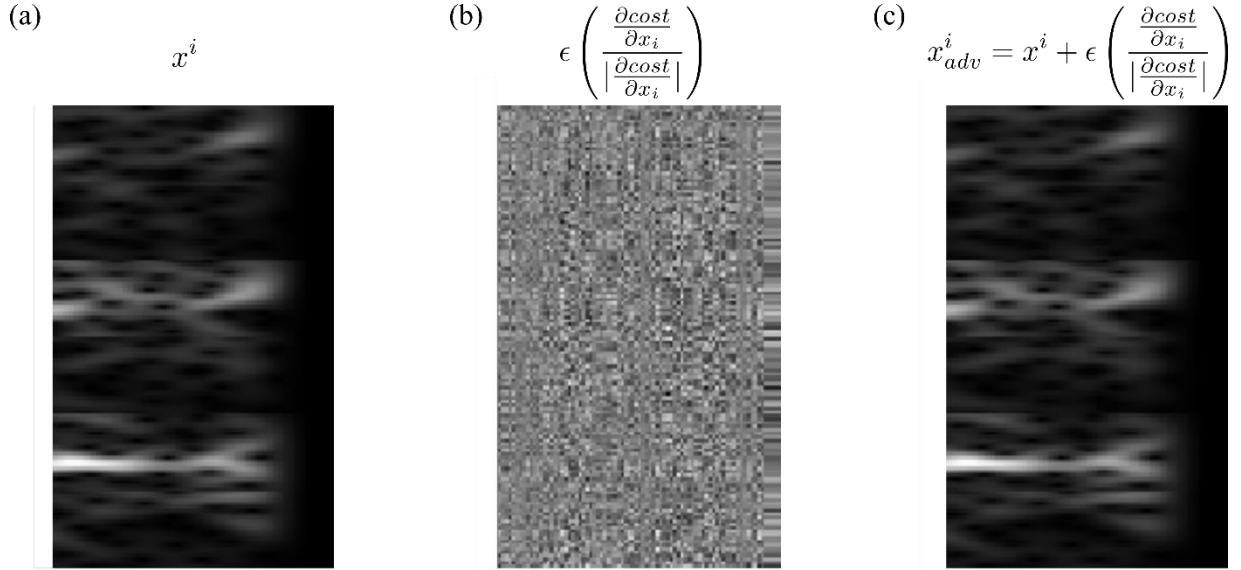


**Figure 12:** The effect of perturbations provided by gradient norm method on the correctly classified input. (a), an input which is correctly classified by an employed classification algorithm (Skip-Net). (b), the perturbations generated using gradient norm method. (c), the resultant input generated by adding the perturbations into the original input.

The perturbations offered by gradient sign method (Goodfellow, Shlens, & Szegedy, 2014) is shown in **Figure 13**. Here, the magnitude of the perturbation is either 1 or -1. As a result, the importance of each feature is disregarded. The perturbation is either white (1) or black (-1) as shown in **Figure 13 (b)**. On the other hand, the most perturbations lie in the gray area for gradient norm method (see **Figure 12 (b)**). Here, only the most important features, which are only a few features, are either black or white. Therefore, we considered only the gradient norm for data augmentation and for the above stated analysis.

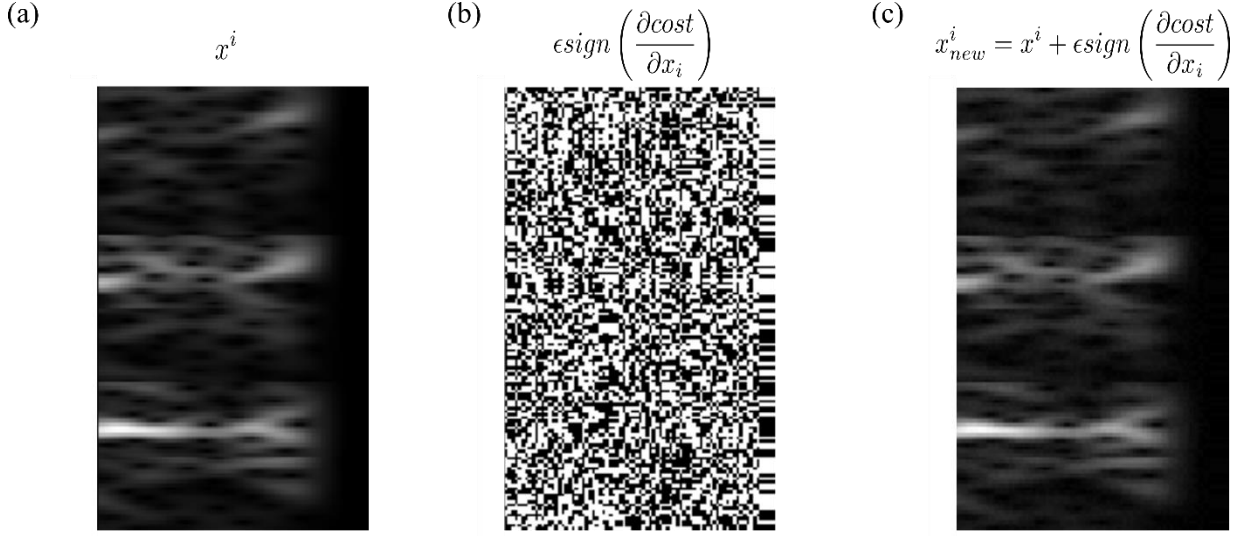


**Figure 13: The effect of perturbation provided by gradient sign method on the correctly classified input.** (a), an input which is correctly classified by an employed classification algorithm (Skip-Net). (b), the perturbations generated using gradient sign method. (c), the resultant input generated by adding the perturbations into the original input.

### Pockets of adversarial inputs

Additionally, we determine the pockets of adversarial inputs for each subject of BCI competition IV dataset 2b. We defined pockets of adversarial input in equation (6). The term  $\beta$  in equation (6) defines the minimum required perturbations, such that the difference between two inputs (original input and perturbed input) remains visually indistinguishable but the perturbed inputs successfully fool the employed classification algorithm. The value of  $\beta$  is (0.01) determined empirically. **Table 8** shows the adversarial pockets for each subject of BCI competition IV dataset 2b. It can be seen from **Table 8** that subject 1 (S1) has zero inputs that were misclassified by the classification algorithm when perturbed by using the factor of  $\beta = 0.01$  and all the perturbed inputs were augmented with the original unperturbed inputs to enhance the training dataset whereas, subject 5 (S5) has 273 examples that when perturbed, were misclassified by the classification algorithm and only the remaining perturbed inputs were augmented with original unperturbed inputs to enhance the training data. The reason for S1 to have 0 adversarial pockets is that the inputs are further away from the decision boundary such that even after the perturbation, the inputs remained on the correct side of the boundary. The reason for S5 to have 273 adversarial pockets is that the inputs are closer to the decision boundary such that after slight perturbation, the inputs are shifted to the other side of the boundary.

**Table 8:** Adversarial pockets for each subject for beta = 0.01 for BCI competition IV dataset 2b.

<b><math>\beta = 0.01</math></b>									
Subjects	S1	S2	S3	S4	S5	S6	S7	S8	S9
Total examples	1216	1302	1302	1872	1601	1106	1255	1199	1240
Adv. Pockets	0	1	2	38	273	86	174	94	83

## Discussion and summary

In this study, an algorithm for feature formation called anchored-STFT is presented. The decoding performance of EEG-MI is improved on two publicly available datasets by using the anchored-STFT and a novel architecture of CNN called Skip-Net. In addition, we proposed a data augmentation technique to generate new training examples from the existing examples in the training dataset. The proposed data augmentation is called GNAA. We showed that the decoding accuracy on the dataset used in this study is further improved by adding the augmented data generated by GNAA in the decoding loop. Lastly, we investigated the existence of adversarial inputs in BCI applications. To the best of our knowledge, there is no other study that has investigated the existence of adversarial inputs in neural data.

The proposed anchored-STFT is inspired by wavelets transform (DebnathJean & Antoine, 2003) and Faster RCNN (Ren S. , He, Girshick, & Sun, 2015). Wavelets transform scales and dilates the mother wavelet. It then slides these scaled and dilated wavelets across the time-domain signal to generate a scalogram in the frequency domain. However, anchored-STFT uses anchors of different lengths. It slides these anchors across the time-domain signal to transform it to a spectrogram with

different time-frequency resolution in frequency domain. Anchored-STFT generates one spectrogram for each anchor whereas the wavelet transform produces only one scalogram for all the used scales and translation factors. The anchored-STFT also addresses the limitation of standard STFT by minimizing the trade-off between temporal and spectral resolution. Anchored-STFT uses anchors of different lengths to extract segments of corresponding lengths from the time-series signal and applies Fourier transform to each extracted segmented signal. Henceforth, temporal, and spectral resolution is optimized.

Additionally, we proposed a novel architecture for the classification of MI-EEG signals which contains one skip connection, hence named Skip-Net. Our Skip-Net comprises two convolutional layers. The first convolutional layer uses filters that convolve on the time axis and extracts frequency domain features along the time axis, whereas the second convolutional layer extracts the time-domain features. We used the additive skip connection to combine the extracted frequency and time domain features to prevent the loss of any information which in turn improved the classification performance of the Skip-Net compared to other classifiers.

The performance of deep learning algorithms is also dependent on the number of training examples. Therefore, we proposed a data augmentation technique to increase the amount of training examples. The proposed data augmentation algorithm used the objective function of the previously trained model, which is trained on the original training examples. Then, the new inputs are crafted by perturbing the original training examples towards the direction of the decision boundary of the classifier. The direction of perturbation of each new input is determined by calculating the gradient of the optimized objective with respect to its original input as defined in equation (5). The magnitude of the perturbation is kept small and defined by factor epsilon (see equation (5)).

In this study we showed that the Skip-Net trained on inputs generated by anchored-STFT (with and without data augmentation) yielded better classification performance in terms of accuracy for session-to-session classification task compared to the classifiers trained on inputs generated by

standard STFT as presented in (Tabar & Halici, 2017). In session-to-session classification task on BCI competition IV dataset 2b, (Tabar & Halici, 2017) split the training data sessions into training and evaluation datasets. Two training sessions (01T and 02T) were used for training whereas, the remaining third training session (03T) was used for the evaluation of the algorithms. We used the same data splitting technique for the comparison of our proposed pipeline with the algorithms proposed in (Tabar & Halici, 2017). The performance comparison of both types of classifiers for session-to-session classification task on BCI competition IV dataset 2b is evident in **Table 2**, which shows that the anchored-STFT based classifier (Skip-Net with GNAA) improved the classification accuracy results by 2.9 %, 5.6 % and 7.7 % compared to CNN-SAE, CNN, and SAE classifiers, respectively which are based on the standard STFT. However, anchored-STFT + Skip-Net without GNAA improved the classification accuracy results by 1.8 %, 4.5 % and 6.6 %, when compared with CNN-SAE, CNN, and SAE methods, respectively.

However, BCI competition IV dataset 2b has separate training (01T, 02T and 03T) and evaluation datasets (04E and 05E). A fair comparison of algorithms requires to use the training dataset for training and evaluation dataset for evaluation as provided by the organizers of the BCI competition IV dataset 2b. Henceforth, we provided an additional analysis and compared the best two algorithms of (Tabar & Halici, 2017) with the anchored-STFT + Skip-Net in combination with GNAA on session-to-session classification task, where the training session (01T, 02T and 03T) are used for training and the evaluation sessions (04E and 05E) are used for evaluation of the performance of the algorithms. The results of the comparison of the algorithms are shown in **Table 9**. Here, the proposed pipeline provides the improvement in classification accuracy by 4.9% and 5.5 % compared to CNN and CNN-SAE respectively. The architecture of CNN-SAE as proposed by (Tabar & Halici, 2017) has 6 autoencoders, which in our opinion is quite deep and redundant for data available in BCI competition IV dataset 2b. It also could cause the vanishing gradient problem which we tried to avoid by introducing a skip connection. We also briefly investigated the performance of the shallow architecture of CNN-SAE which included only two autoencoders which were trained only for 50 epochs each and jointly finetuned for 400 epochs. The performance of the shallow architecture of CNN-SAE was roughly the same and slightly better than standard CNN-SAE architecture for some subjects.

**Table 9:** Comparison of accuracy results generated by CNN, SAE, CNN-SAE (Tabar & Halici, 2017) and anchored-STFT + Skip-Net with/without GNAA for session-to-session classification task (trained on 01T, 02T and 03T sessions and evaluated on 04E and 05E sessions) of dataset 2b from BCI competition IV.

Subjects	CNN	CNN-SAE	anchored-STFT + Skip-Net (GNAA)
S1	71.3	66.6	<b>74.7</b>
S2	<b>58.2</b>	54.3	55.0
S3	53.8	56.6	<b>59.1</b>
S4	95.9	95.6	<b>96.9</b>
S5	80.6	80.3	<b>92.2</b>
S6	79.4	80.6	<b>87.2</b>
S7	74.4	71.9	<b>81.9</b>
S8	89.1	90.6	<b>93.4</b>
S9	80.9	82.5	<b>87.8</b>
Average	<b>76.0</b>	75.4	<b>80.9</b>

We also compared the performance of anchored-STFT with other existing feature extraction algorithms. In (Ang et al, 2012), the FBCSP algorithm is proposed, which was the winner algorithm in the BCI competition IV for dataset 2b. Here, we showed in **Table 3** and **Table 4**, that anchored-STFT based decoder (Skip-Net with GNAA) outperformed FBCSP on the same dataset by 3.2 % and 3.6 % in terms of kappa value for session-to-session classification task and single-trial classification task, respectively.

Our anchored-STFT based classifier (Skip-Net with GNAA) also gave the best classification results on dataset III from BCI competition II both in terms of accuracy and kappa value. It outperformed (see **Table 6**) the standard STFT based classifier (CNN-SAE) (Tabar & Halici, 2017) and the winner algorithm (Lemm, Schäfer, & Curio, 2004) of the competition by 0.70 % and 1.4 %, respectively in terms of accuracy and 1.75 % and 3.9 %, respectively in terms of kappa values. We showed in the **Results** section that the presented algorithms enable improvements compared to the results presented (Tabar & Halici, 2017), (Keng Ang, Yang Chin, Wang, Guan, & Zhang, 2012), (Suk & Seong-Whan, 2011), (Gandhi, et al., 2011), (Shahid, Sinha, & Prasad, 2010) and (Lemm, Schäfer, & Curio, 2004).

BCI competition IV dataset 2b consists of the EEG-MI data of nine subjects. Results shown in this and the following studies (Tabar & Halici, 2017), (Keng Ang, Yang Chin, Wang, Guan, & Zhang, 2012), (Suk & Seong-Whan, 2011), (Gandhi, et al., 2011), (Shahid, Sinha, & Prasad, 2010) and (Lemm, Schäfer, & Curio, 2004) indicate that the classification of the EEG-MI data of subjects 2 and 3 posed difficulty and performance of all the compared algorithms remains suboptimal on the data of these two subjects. Henceforth, we analyzed the data of these subjects more deeply. We calculated the mean spectra of both classes for all the trials using anchored-STFT and compared them with the mean spectra of subject 4 (see **Figure 14**). We selected subject 4 because it has the highest classification accuracy among all subjects. The difference between the mean spectra of left- and right-hand MI of subject 4 is very clear in **Figure 14** (c). There is an increase of activation in C3 electrode and decrease of activation in C4 electrode for subject 4's left-hand MI, whereas there is decrease of activation in C3 electrode and increase of activation in C4 electrode for subject 4's right-hand MI. However, this difference is not very clear for subjects 2 and 3 (see **Figure 14** (a) and (b)). To validate this difference, we also calculated the normalized cross correlation between the mean spectra of left- and right-hand MI of subjects 2 and 3. Peak normalized cross correlation of 1.0 is obtained if an image is correlated with itself, indicating the absolute similarity between them, however a low peak normalized cross correlation is obtained if two different images are correlated. We obtained the peak normalized cross correlation of 0.99 for subjects 2 and 3 which clearly shows that the mean spectra of both classes of subjects 2 and 3 are highly correlated which is also evident from the classification accuracy of these subjects.

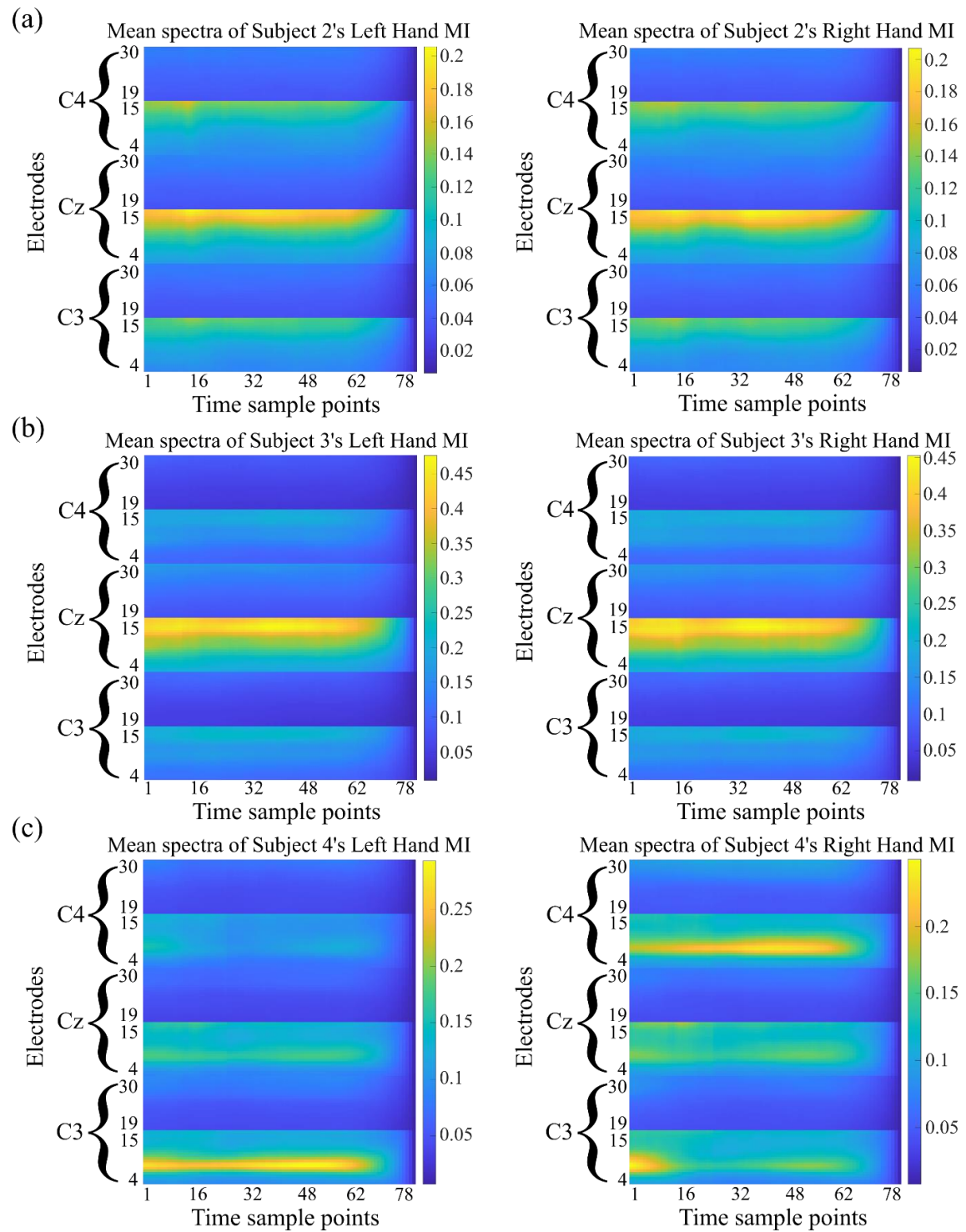


**Figure 14:** Mean spectra of left- and right-hand MI of subjects 2,3 and 4. Difference between the mean spectra of subject 4 is clear for both classes. Whereas the difference between the spectra of subjects 2 and 3 is not clear for both classes

Lastly, we investigated the existence of adversarial inputs in neural data. The existence of adversarial inputs in computer vision has already been studied in (Goodfellow, Shlens, & Szegedy, 2014; Szegedy, et al., 2014) However, their existence in neural data has not been previously investigated. Here, we investigated the existence of adversarial inputs for neural data and introduced a novel method for crafting adversarial inputs. We named the novel method for crafting adversarial inputs as gradient norm method (GNAA). The gradient norm method is also compared with one existing method called gradient sign method (Goodfellow, Shlens, & Szegedy, 2014; Szegedy, et al., 2014) The perturbations applied by the two methods are significantly different as shown in **Figure 7**. The perturbation applied by the gradient norm method is shown in **Figure 7(a)** and the perturbation applied by gradient sign method is shown in **Figure 7(b)**. The perturbation applied by gradient norm method carefully selects the features that are important for the employed classification algorithm as shown in **Figure 7(a)**. However, the perturbation applied by the gradient sign method seems to be random (see **Figure 7(b)**). The randomness lies in the perturbation because of the signum operator in equation (6). The signum operator maps all the values of zero and above to 1 and the values less than zero to -1 in the perturbation matrix (see **Figure 7(b)**). As a result, the perturbation matrix is filled with values of either 1 or -1 and the importance of each feature is disregarded.

This research mainly focused on developing a better feature extraction technique (anchored-STFT) which addresses the short comings of standard STFT. Producing state-of-the-art results on the datasets used in this research is beyond the scope of this study. In addition, this study focused on investigating the existence of adversarial inputs in the domain of BCI and the use of adversarial inputs for generating more training data (GNAA). Henceforth, we compared the performance of our pipeline only with STFT based classifiers and the winner algorithm of the competitions. The results reported in this study can further be improved by employing more sophisticated data augmentation techniques and deep hybrid architectures of neural networks as presented in (Dai, Zhou, Huang, & Wang, 2020).

The current version of anchored-STFT constructs a separate feature matrix for each defined anchor and each feature matrix is provided to the classifier. Then, the voting strategy is applied to take the final decision. In the future, we are aiming to construct a single but more meaningful feature matrix from all the anchors. We believe that if all the necessary information is provided at once, it can increase the generalization quality of deep learning models. As a result, the computational cost of the proposed pipeline can also be reduced. Here, we briefly investigated the existence of adversarial inputs in neural data. However, more thorough investigation is required. Therefore, in future we are aiming to extract adversarial inputs created by different methods and try to train a more robust classifier by training it on data that has more variability.

## Acknowledgement

This work is supported by the Ministry of Economics, Innovation, Digitization and Energy of the State of North Rhine-Westphalia and the European Union, grants GE-2-2-023A (REXO) and IT-2-2-023 (VAFES).

# Bibliography

A. Mousavi, E., J. Maller, J., B. Fitzgerald, P., & J. Lithgow, B. (2011). Wavelet Common Spatial Pattern in asynchronous offline brain computer interfaces. *Biomedical Signal Processing and Control*, 121-128.

Aflalo, T., Kellis, S., Klaes, C., Lee, B., Shi, Y., Pejsa, K., . . . A Andersen, R. (2015). Decoding motor imagery from the posterior parietal cortex of a tetraplegic human. *Science*, 906-910.

Ajiboye, A. B., Willett, F. R., Young, D., Memberg, W. D., A Murphy, B., P Miller, J., . . . Kirsch, R. F. (2017). Restoration of reaching and grasping movements through brain-controlled muscle stimulation in a person with tetraplegia: a proof-of-concept demonstration. *The Lancet*, 389(10081), 1821-1830. doi:10.1016/S0140-6736(17)30601-3

Allen, J., & Lawrence , R. (1977). A unified approach to short-time Fourier analysis and synthesis. *Proceedings of the IEEE* 65.11, (pp. 1558-1564).

An, X., Kuang, D., Guo, X., Zhao, & He, L. (2014). A Deep Learning Method for Classification of EEG Data Based on Motor Imagery. *Intelligent Computing in Bioinformatics*, [https://doi.org/10.1007/978-3-319-09330-7\\_25](https://doi.org/10.1007/978-3-319-09330-7_25).

Bashivan, P., Rish, I., Yeasin, M., & Codella, N. (2015). Learning Representations from EEG with Deep Recurrent-Convolutional Neural Networks. *arXiv*, <https://arxiv.org/abs/1511.06448>.

Choi, J., Kim, S., Ryu, R., Kim, S., & Sohn, J. (2018). Implantable Neural Probes for Brain-Machine Interfaces - Current Developments and Future Prospects. *Experimental Neurobiology*, 27(6), 453-471. doi:10.5607/en.2018.27.6.453

Cortes, C., & Vapnik, V. (1995). Support-vector networks. *Machine Learning*, 273–297.

Dai, G., Zhou, J., Huang, J., & Wang, N. (2020). HS-CNN: a CNN with hybrid convolution scale for EEG motor imagery classification. *Journal of Neural Engineering*, 17(016025). doi:10.1088/1741-2552/ab405f

DebnathJean, L., & Antoine, J.-P. (2003). *Wavelet Transforms and Their Applications*. Louvain-la-Neuve: Physics Today.

Firat Ince, N., Arica, S., & Tewfik, A. (2006). Classification of single trial motor imagery EEG recordings with subject adapted non-dyadic arbitrary time-frequency tilings. *Journal of Neural Engineering*, doi: 10.1088/1741-2560/3/3/006.

Fukunaga, K. (2013). *Introduction to Statistical Pattern Recognition*. Elsevier.

Gandhi, V., Arora, V., Behera, L., Prasad, G., Coyle, D., & McGinnity, T. (2011). EEG denoising with a recurrent quantum neural network for a brain-computer interface. *In The 2011 International Joint Conference on Neural Networks. IEEE.*, (pp. 1583-1590).

Goodfellow, I. J., Shlens, J., & Szegedy, C. (2014). Explaining and Harnessing Adversarial Examples. *arXiv*, arXiv:1412.6572.

Graimann, B., Allison, B., & Pfurtscheller, G. (2010). *Brain–Computer Interfaces: A Gentle Introduction*. Berlin: Springer.

Grosse-Wentrup, M., & Buss, M. (2008). Multiclass Common Spatial Patterns and Information Theoretic Feature Extraction. *IEEE Transactions on Biomedical Engineering*, 1991 - 2000.

He, K., Zhang, X., Ren, S., & Sun, J. (2016). Deep Residual Learning for Image Recognition. *IEEE Conference on Computer Vision and Pattern Recognition (CVPR)*, (pp. 770-778).

Issar, D., C. Williamson, R., B. Khanna, S., & A. Smith, M. (2020). A neural network for online spike classification that improves decoding accuracy. *Journal of Neurophysiology*, 123(4), 1472-1485. doi:<https://doi.org/10.1152/jn.00641.2019>

Jirayucharoensak, S., Pan-Ngum, S., & Israsena, P. (2014). EEG-Based Emotion Recognition Using Deep Learning Network with Principal Component Based Covariate Shift Adaptation. *The Scientific World Journal*, <https://doi.org/10.1155/2014/627892>.

Kellis, S., Miller, K., Thomson, K., Brown, R., House, P., & Greger, B. (2010). Decoding spoken words using local field potentials recorded from the cortical surface. *Journal of neural engineering*, 056007.

Keng Ang, K., Yang Chin, Z., Wang, C., Guan, C., & Zhang, H. (2012). Filter bank common spatial pattern algorithm on BCI competition IV Datasets 2a and 2b. *Frontier in Neuroscience*, <https://doi.org/10.3389/fnins.2012.00039>.

Klaes, C., Kellis, S., Afalo, T., Lee, B., Kelsie, P., Shanfield, K., . . . A. Andersen, R. (2015). Hand Shape Representations in the Human Posterior Parietal Cortex. *The Journal of Neuroscience*, 15466–15476.

Kübler, A., Furdea, A., Halder, S., Hammer, E. M., Nijboer, F., & Kotchoubey, B. (2009). A brain-computer interface controlled auditory event-related potential (p300) spelling system for locked-in patients. *Annals of the New York Academy of Sciences*, doi: 10.1111/j.1749-6632.2008.04122.x. .

Leeb, R., Lee, F., Keinrath, C., Scherer, R., Bischof, H., & Pfurtscheller, G. (2007). Brain-computer communication: motivation, aim, and impact of exploring a virtual apartment. *IEEE Trans. Neural Syst. Rehabil. Eng.*, 15(4):473–82.

Lemm, S., Schäfer, C., & Curio, G. (2004). BCI competition 2003-data set III: probabilistic modeling of sensorimotor  $\mu$  rhythms for classification of imaginary hand movements . *IEEE Trans. Biomed. Eng.* 51, 1077- 80.

Li , F., He, F., Wang, F., Zhang, D., Xia, Y., & Li, X. (2020). A Novel Simplified Convolutional Neural Network Classification Algorithm of Motor Imagery EEG Signals Based on Deep Learning. *Applied Sciences*. doi:[10.3390/app10051605](https://doi.org/10.3390/app10051605)

Müller-Gerking, J., Pfurtscheller, G., & Flyvbjerg, H. (1999). Designing optimal spatial filters for single-trial EEG classification in a movement task. *Clinical Neurophysiology*, 787-798.

Nicolas-Alonso, L. F., & Gomez-Gil, J. (2012). Brain Computer Interfaces, a Review. *Sensors*, <https://doi.org/10.3390/s120201211>.

Nielsen, T. D., & Jensen, F. V. (2001). *Bayesian Networks and Decision Graphs*. Springer-Verlag New York.

Pfurtscheller, G., & FH Lopes Da Silva. (1999). Event-related EEG/MEG synchronization and desynchronization: basic principles. *Clinical neurophysiology* 110.11, 1842-1857.

Pfurtscheller, G., & Lopes da Silva, F. (1999). Event-related EEG/MEG synchronization and desynchronization: basic principles. *Clinical Neurophysiology*, 1842-1857.

Ramoser, H., Muller-Gerking, J., & Pfurtscheller, G. (2000). Optimal spatial filtering of single trial EEG during imagined hand movement. *IEEE Transactions on Rehabilitation Engineering*, DOI: 10.1109/86.895946.

Ren, S., He, K., Girshick, R., & Sun, J. (2015). Faster R-CNN: Towards Real-Time Object Detection with Region Proposal Networks. *arXiv*, arXiv:1506.01497.

Ren, S., He, K., Girshick, R., & Sun, J. (2017). Faster R-CNN: Towards Real-Time Object Detection with Region Proposal Networks. *IEEE Transactions on Pattern Analysis and Machine Intelligence*, 39(6), 1137-1149. doi:10.1109/TPAMI.2016.2577031.

Ren, Y., & Wu, Y. (2014). Convolutional deep belief networks for feature extraction of EEG signal. *International Joint Conference on Neural Networks (IJCNN)* (p. DOI: 10.1109/IJCNN.2014.6889383). Beijing: IEEE.

Ren, Y., & Wu, Y. (2014). Convolutional deep belief networks for feature extraction of EEG signal. *International Joint Conference on Neural Networks (IJCNN)* (p. 10.1109/IJCNN.2014.6889383). Beijing: IEEE.

Rezaei Tabar, Y., & Halici, U. (2017). A novel deep learning approach for classification of EEG motor imagery signals. *Journal of Neural Engineering*, doi: 10.1088/1741-2560/14/1/016003.

Saif-ur-Rehman, M., Ali, O. D., Lienkämper, R., Metzler, M., Parpaley, Y., Wellmer, J., . . . Klaes, C. (2020). SpikeDeep-Classifier: A deep-learning based fully automatic offline spike sorting algorithm. *Journal of Neural Engineering*, <https://doi.org/10.1088/1741-2552/abc8d4>.

Saif-ur-Rehman, M., Lienkämper, R., Parpaley, Y., Wellmer, J., Liu, C., Lee, B., . . . Klaes, C. (2019). SpikeDeeptector: a deep-learning based method for detection of neural spiking activity. *Journal of Neural Engineering*, 16 5. doi:<https://doi.org/10.1088/1741-2552/ab1e63>

Schlögl, A. (2003). *Outcome of the BCI-competition 2003 on the Graz data set*. Berlin: Graz University of Technology.

Schlögl, A. (2003). *Outcome of the BCI-competition 2003 on the Graz data set*. Retrieved from [bbsci.de: http://bbsci.de/competition/ii/results/TR\\_BCI2003\\_III.pdf](http://bbsci.de/competition/ii/results/TR_BCI2003_III.pdf)

Schlögl, A., Flotzinger, D., & Pfurtscheller, G. (1997). Adaptive autoregressive modeling used for single-trial EEG classification. *Biomedizinische Technik/Biomedical Engineering* 42.6, 162-167. doi:10.1515/bmte.1997.42.6.162

Schlögl, A., Lee, F., Bischof, H., & Pfurtscheller, G. (2005). Characterization of four-class motor imagery EEG data for the BCI-competition 2005. *Journal of Neural Engineering*, <https://doi.org/10.1088/1741-2560/2/4/L02>.

Sejdić, E., Djurović, I., & Jiang, J. (2009). Time–frequency feature representation using energy concentration: An overview of recent. *Digital Signal Processing*, <https://doi.org/10.1016/j.dsp.2007.12.004>.

Shah, Z. H., Müller, M., Wang, T.-C., Scheidig, P. M., Schneider, A., Schüttelz, M., . . . Schenck, W. (2020). Deep-learning based denoising and reconstruction of super-resolution structured illumination microscopy images. *bioRxiv*. doi: <https://doi.org/10.1101/2020.10.27.352633>

Shahid, S., Sinha, R., & Prasad, G. (2010). A bispectrum approach to feature extraction for a motor imagery based brain-computer interfacing system. *18th European Signal Processing Conference. IEEE, 2010*, (pp. 1831-1835).

Suk, H.-I., & Seong-Whan, L. (2011). Data-driven frequency bands selection in EEG-based brain-computer interface. *International Workshop on Pattern Recognition in NeuroImaging. IEEE, 2011*, 25-28.

Szegedy, C., Zaremba, W., Sutskever, I., Bruna, J., Erhan, D., Goodfellow, I., & Fergus, R. (2014). Intriguing properties of neural networks. *arXiv*, arXiv:1312.6199.

Tabar, Y. R., & Halici, U. (2017). A novel deep learning approach for classification of EEG motor imagery signals. *Journal of Neural Engineering*, DOI: 10.1088/1741-2560/14/1/016003.

Wulsin, D. F., Gupta, J. R., Mani, R., Blanco, J. A., & Litt, B. (2011). Modeling electroencephalography waveforms with semi-supervised deep belief nets: fast classification and anomaly measurement. *Journal of Neural Engineering*, doi: 10.1088/1741-2560/8/3/036015.

Yang, H., Sakhavi, S., K. Ang, K., & Guan, C. (2015). On the use of convolutional neural networks and augmented CSP features for multi-class motor imagery of EEG signals classification. *Annual International Conference of the IEEE Engineering in Medicine and Biology Society (EMBC)* (pp. 2620-2623). Milan: IEEE.

